NATIONAL UNIVERSITY OF SCIENCE AND TECHNOLOGY POLITEHNICA BUCHAREST
DOCTORAL SCHOOL OF ELECTRICAL ENGINEERING

Ph.D. THESIS

AGING OF POWER TRANSFORMER MINERAL OIL UNDER HIGH STRENGTH ELECTRIC FIELD AND PARTIAL DISCHARGES

-SUMMARY-

Scientific Coordinator,

Prof. Dr. Eng. Laurențiu Marius DUMITRAN

Author,

Eng. Andrei MANEA

BUCHAREST

2024

Contents

Key words: mineral oil, power transformers, high strength electric field and partial discharges, accelerated aging, electric conductivity, activation energy, mineral oil conductivity, mobility of charge carriers, activation energy.

CHAPTER 1

INTRODUCTION

This PhD thesis addresses the field of dielectric materials for power transformers, focusing on the development of a method for accelerated aging of mineral oil under the action of high strength electric field and partial discharges for different aging times.

Most high and extremely high-voltage power transformers still use mineral oil and cellulose paper as insulation, despite recent developments promoting innovative insulation techniques [1.1, 1.2]. Under typical operating conditions, power transformers (PTs) main characteristics change, and their oil and paper components gradually degrade.

The topic of insulation systems for power transformers has been extensively researched, covering a wide range of specific issues. The majority of these concentrate on the analysis of the mechanisms underlying the deterioration of the insulation's constituent parts (oils and paper), as well as on effective diagnostic tools and techniques for evaluating the insulation system's state. Conventional diagnostic techniques can offer broad insights into the overall state of the paper-oil insulation system by measuring insulation resistance, absorption and resorption currents, returning voltage, etc. [1.3-1.5]. Other techniques rely on the physio-chemical examination of oil samples that may be obtained from the transformer tank and are more accessible than paper samples. The most commonly used techniques among these are dielectric spectroscopy, water content, furan content, and the study of dissolved gases [1.6, 1.7]. The physio-chemical characteristics of oil and paper are generally thought to undergo significant changes due to thermal stress [1.8].

However, there are still questions about how the high-strength electric field affects the insulation system's components, despite the fact that the processes of oil-paper insulation's thermal aging are well understood. These ambiguities are particularly accentuated in high and extremely high voltage transformers (PTs) because of the localized concentration of the electric field caused by specific micro-defects or impurities, potential partial electric discharges (PDs), and localized oil breakdown, which rapidly decrease the oil's dielectric properties.

The subject of determining and measuring PD levels in high-voltage electrical equipment is covered in an extensive amount of literature. The effects of this phenomenon on the insulating state are examined but in relatively few instances. Thus, there haven't been many detailed studies done on how the high electric field and PDs affect the dielectric characteristics of oil-paper insulation in power transformers. Thus, the main objective of this Ph.D. thesis was to develop an experimental laboratory method for accelerated aging of mineral transformer oil subjected to a high-strength electric field and partial discharges in the oil volume. By doing this, we attempted to replicate as closely as we could the real-life conditions that arise inside the power transformer due to the variable regimes that it operates under.

The ASTM D 6180-05 [1.9] standardized test for evaluating insulating oils of petroleum origin for stability under electric discharge situations only gives specific details about the behavior of the oil when electric discharges happen at its surface and not in its volume. Thus, to accomplish the intended objective, an original aging cell that enables the aging of transformer oil samples in liquid volume across a certain time period was designed and fabricated. The aging cell's implementation considered the opportunities and limitations of component manufacturing, replication, and supplying.

Another important objective of the thesis was to study the influence of partial discharges and high-strength electric fields on dielectric properties by evaluating diagnostic factors using the dielectric spectroscopy method. Dielectric spectroscopy is a preferred tool in the field of electro-insulating materials, being extremely effective for studying the structure and dynamics of insulation systems and allowing the evaluation of intrinsic phenomena in them. The acquired results highlight how fast and significant the influence of electrical aging is on the dielectric properties of aged mineral oil, providing us some insight regarding the conduction and polarization processes in this material. It's worth noting that aged mineral oil can undergo notable changes in its dielectric properties within only a few hours.

Chapter 1 covers the transformer's role and importance in the electrical grid, as well as specific conditions and operating regimes that contribute to the rapid deterioration of the transformer insulating system. This chapter also presents the purpose and organization of the thesis, along with the justification and objective of the study.

Chapter 2 presents a brief description of the power transformer's components as well as constructive solutions. Materials utilized for executing the transformer insulation system are reviewed, with an emphasis on their benefits and disadvantages determined by their composition and characteristics. It also revealed the rationale for the study's main focus, which is mineral oil, given that Kraft paper insulation and mineral oil are still widely used in the construction of power transformers.

Chapter 3 presents the stresses that power transformer insulation systems experience during operation and provides a discussion of the degradation reactions that take place. Regarding operating and maintenance strategies, these can be developed and improved to ensure proper functionality and extend the lifespan of transformers. That can be achieved by identifying the most harmful stress factors and chemical reactions caused by the high-strength electric field or heat. Thus, by recognizing these factors, appropriate measures can be taken to mitigate their effects and ensure the transformer's longevity.

Chapter 4 describes the diagnostic techniques (electrical, chemical, thermal, and acoustic) utilized on a broad scale, with a particular emphasis on the electrical methods employed in this research. The advantageous aspects of these techniques for achieving the purpose are therefore discussed, highlighting dielectric methods using analysis of dielectric responses in time and frequency.

Chapter 5 covers the major characteristics of the aging cell as well as the geometrical description of the metallic electrode in it. In addition, the mathematical model for the computation, the material and specific properties, and the associated numerical models for the three and six-disc metallic electrodes are described. Also, the aging cell's final configuration and design are established, along with some process steps, as part of the method preparation.

Based on the indication given by the numerical calculation and the useful experimental findings, the six-disk electrode has been selected to undergo laboratory testing and will be used for accelerated oil aging to fulfill the study's objectives.

Additionally, visual experimental results are shown, emphasizing the phenomena of electrical discharging, the bubbling process, and the oil's color change. Regarding the suggested methodology and its conditions, the outcome validated that the method is reliable and effective, generating consistent outcomes and enabling the generation of gas bubbles within the oil volume, which subsequently triggers significant visible partial discharges.

Chapter 6 deals with the experimental results and the methods utilized to assess the results of the experiments. Accordingly, a thorough explanation of the dielectric spectroscopy method (time and frequency domain), along with a closer examination of the main diagnostic factors (as well as the complementary ones) utilized in the assessment of oil characteristics, is presented. An examination from the perspective of complex relative conductivity was emphasized to identify the conduction processes occurring in different stages of oil degradation. We also explore the hypothesis of generating charge carriers from different species that may be more mobile and more easily activated in the conduction process to explain the significant rise in conductivity, which is attributed, on the other hand, to the increase in the concentration of free charge carriers. Thus, based on a simplified model, the mean mobility of conduction ions and activation energy were determined for different aging times and temperatures. The obtained result demonstrated the validity of this hypothesis. Therefore, given the existence of these free ions, we can state that the majority of the chemical species in the oil are affected by the continuous process of hydrocarbon molecules fragmenting generated by partial discharges and by the high-strength electric field.

CHAPTER 2

POWER TRANSFORMERS DESIGN AND MATERIALS

This chapter discusses the main elements of the power transformer, as well as constructive solutions. The materials utilized for constructing the transformer insulation system are reviewed with a focus on the benefits and drawbacks that come from their composition and attributes. It also explains why the study's primary emphasis was mineral oil, since high power transformer construction still frequently uses both mineral oil and kraft paper for insulation.

2.1 Power transformers constructive solutions and components

Manufacturers construct power transformers in varying ways, but the basic structure remains unchanged over time. [2.1]

Generally, there are two transformer types:

- **Dry-types** are frequently insulated with resin and cooled using natural air and possibly cooling fans;
- **Oil -types** are insulated with solid insulation and oil; the winding is cooled by oil.

2.1.1 Magnetic core

The core, which provides the magnetic flux path, is constructed of thin strips of high-permeability silicon steel (laminations) that are electrically separated by a thin, coated layer of insulating material. As a design, there are two construction types of magnetic core used in power transformers: core form and shell form; when windings encircle the core, the transformer is known as the core type; when windings are framed by the core, the transformer is called the shell type [2.2].

2.1.2 Transformer windings

A transformer's winding is composed of insulated conductors, typically copper or aluminum that is wrapped around the magnetic core. The electromagnetic field requires the winding to be strongly consolidated and properly cooled to sustain the working conditions. Although aluminum is lighter and less costly in general, a bigger cross-section of aluminum conductors is required to carry a current with comparable performance to copper; therefore, copper is the chosen and preferred material for winding conductors.

In practice, stranded copper with a rectangular section is utilized for high-power transformers, whereas wire or foil conductors are used for low-power transformers. [2.1]

2.1.2.1 Power transformer windings components

A power transformer's phase (electrically) has two electrical coils, one called the primary winding and the other known as the secondary winding. The two coils are not electrically connected, surrounding only the same magnetic circuit (magnetic core), they are only magnetically coupled through the common core, which transfers electrical energy from one coil to the other. Thus, the purpose of secondary windings is to transmit electrical power by converting magnetic flux. [2.3]

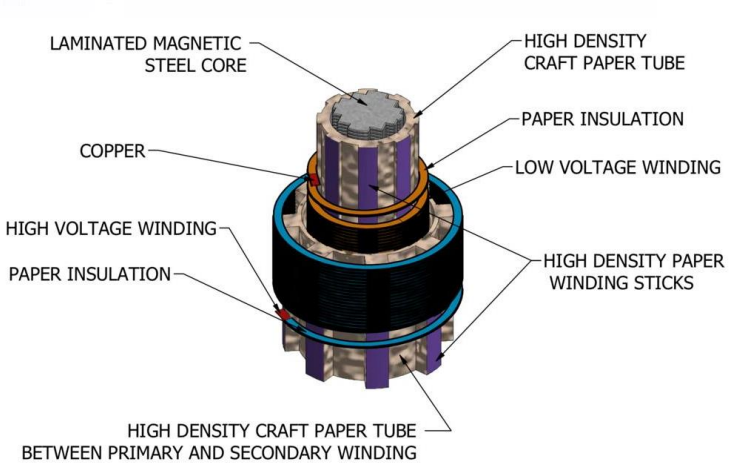

Fig. 2.1. Winding section of a power transformer.

The insulation system of a power transformer depends on the construction type (dry or in oil) and the voltage level of its two windings. Fig. 2.1 shows a schematic diagram of a winding phase from a power transformer.

a b

Fig. 2.2. (a) Paper-insulated rectangular copper wire (single & multiple), (b)- Power transformer insulation kit. [2.4, 2.5]

The basic components of the power transformer insulation are: copper conductor insulation (i.e., paper) Fig.2.2a, insulated tubes, insulation between high and low voltage winding (primary and secondary winding) Fig.2.2b, insulating passages, fixing wedges, etc. [2.6]

2.2 Power transformer insulation system

Power transformer insulation materials include paper, mineral oil, pertinax, and textile tapes. Significant attempts have been undertaken in the case of power transformers to improve the performance of insulation systems by replacing cellulose paper with different types of paper (e.g., polyamide paper or Nomex) and mineral oil with synthetic oils. [2.6] However, the traditional paper-oil system remains the most cost-effective and reliable choice for power transformers, resulting in the majority of power transformers still utilizing insulating mineral oils and cellulose paper-based insulation systems.

2.2.1 Transformer paper/ Cellulose paper

Since the initial equipment's realization, cellulosic products have served as the raw material for the power transformer's insulating system. The ability to manufacture components with a variety of sizes and forms, strong dielectric qualities, and affordable prices led to the widespread usage of cellulosic products in the electrotechnical industry. [2.7]

Cellulosic insulation serves three primary purposes in the transformer: it provides mechanical support for the windings, acts as an insulator for components working at different voltage rates, and creates cooling ducts for the oil in the cooling circuit. [2.8]

Cellulose is a natural macromolecular material having a linear molecule $(C_6H_{10}O_5)_n$. Molecular chains are organized into similarly structured micelles, or thin tubes, which subsequently form fibrils and cellulose fibers. This structure explains the high-water absorption and high porosity (40–50%) of cellulose materials [2.7]. Cellulose's dielectric characteristics are highly dependent on the density, humidity stage, temperature, and frequency of the electric field, being typically lower than those of compact-structured materials. Since cellulose contains polar molecules, its permittivity and dielectric losses have high (relative) values

The primary source of the changes in cellulose's characteristics is the chemical transformations that occur when the electric field's activity is supported by heat and oxygen. Therefore, oxygen depolymerizes cellulose macromolecules, which deteriorates their mechanical qualities. Additionally, oxygen promotes cellulose's chemical interactions with water, which raises the number of polar groups and ultimately lowers the material's dielectric characteristics. [2.7] Cellulose is impregnated with hydrophobic liquids to increase its dielectric properties and minimize hygroscopicity. As a result, the properties of the impregnated substance determine the characteristics of the cellulose itself. Depending on the density of the paper, the relative permittivity of cellulosic paper ranges from 2.2 to 6.35, and when temperature and paper density rise, the loss factor rises as well.

2.2.2 Transformer oil

In addition to having a strong dielectric characteristic, the oil must enable and support the coil-core assembly's cooling process at an optimal temperature for safe operation. It must also minimize the amount of oxygen that comes into contact with cellulose and other components by filling up the gaps and voids in the insulating material. [2.8] Transformer oil may be broadly classified into four categories: mineral oil, vegetable oil, silicone oil, and synthetic ester oil, depending on the source of the base oil. While synthetic, vegetable, and silicone oils have better thermal properties than mineral oil, they have not been able to replace it due to their high cost and limited availability. Mineral oil is still commonly used today.

2.2.2.1 Mineral oil

The basic technique for extracting mineral oil, which is mostly made up of a blend of aromatic, paraffinic, and naphthenic hydrocarbons, is known as oil refining. Mineral oil has a broad range of applications in the electro-technical field, including power transformer insulation systems and other electrical power equipment like switches and power capacitors, etc.

It is well known that the entire state of the insulation system will be impacted by the oil's performance, as shown by its qualities. [2.9] In addition to the importance of dielectric strength and low viscosity that promote heat transmission and oil flow, from a thermodynamic perspective, it is allowed to operate in a wide range of temperatures with high interfacial tension and a high flash point. Mineral oil has a comparatively low relative permittivity (2.2–2.4); however, when the temperature rises, the oil's dielectric strength changes significantly, and the loss factor rises significantly as a result of the load carriers' high mobility (and subsequent conductivity). [2.7].

CHAPTER 3
AGING FACTORS AND DEGRADATION PROCESSES IN OIL-PAPER INSULATION SYSTEM

This chapter addresses the stresses and degradation reactions in power transformer insulation systems, highlighting harmful factors and chemical reactions caused by high-strength electric fields and heat. Thus, better monitoring, operating, and maintenance techniques can extend the lifespan of transformers by detecting chemical reactions brought on by intense electric fields or heat combined with reduced hazardous stress elements.

3.1 Introduction

Power transformer insulation system configuration must consider electrical, thermal, and mechanical stresses, which are influenced by load, power rates, and transformer design. So as to support electromagnetic efforts, the insulation must mechanically maintain conductive elements and endure heat produced by conductors and magnetic circuits. These stresses, which affect insulation systems when electrical equipment is operating, are also known as **influencing factors** and can cause premature decommissioning of the transformer insulation systems. Influence factors could lead to insulation aging, in which case they are often referred to as **aging factors**, or they may permit the evaluation of insulation states (without altering their state of degradation), in which case they are considered **diagnostic factors** [3.1]. In addition to the major categories of stresses (electric, mechanical, and thermal), a number of extra stresses particular to the environment in which the electrical equipment functions are always considered: Humidity, oxygen in the atmosphere, ultraviolet (UV), and other factors.

3.2 Electrical stress

Variable voltages of different magnitudes, shapes, and durations occur during power transformer operation. The stresses in the transformer insulation system will, without a doubt, be distributed differently based on the component materials, construction solution, and insulation structure. [3.1]

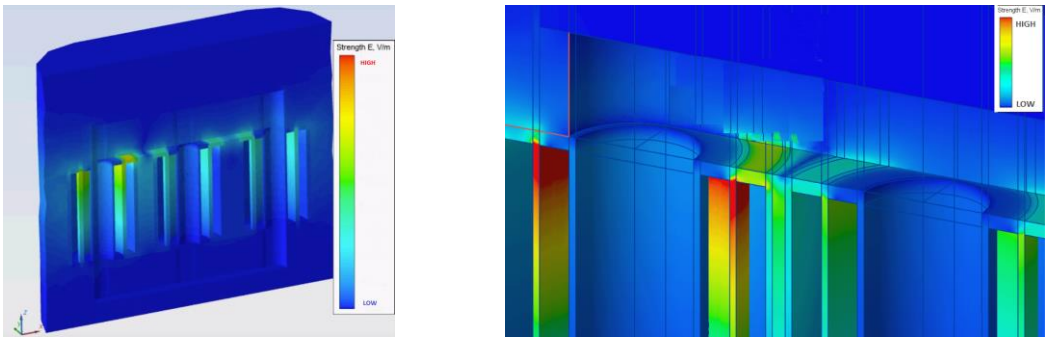

a) b)

Fig. 3.1. (a) Electric field strength in the oil and into power transformer insulation; (b) Electric field stress concentration (coils, core are hidden). [3.2]

The existence of these anomalies in terms of the unequal distribution of electric stresses (Fig. 3.1) motivates this research, whose emphasis is on the effect of mineral oil degradation under the combined influence of a high-strength electric field and partial discharges.

3.2.1 Partial discharges

Partial discharges (PDs) are electrical breakdowns in insulation (that don't bridge electrodes) that generate localized electric stress, causing slow insulation deterioration and power transformer life limitations. [3.3]. A partial breakdown of the surrounding medium results in PD when the electric field is bigger than a threshold value. The PD exhibits transient behavior characterized by pulsing currents with durations ranging from nanoseconds to microseconds. [3.4]. Regarding the severity of the PD phenomenon, we can say that their level can't indicate it because the information is distorted by random and very fast treeing phenomena. Since the complete failure of the insulator destroys it, information about the type of partial discharge generally cannot be retained. [3.5]

The chaotic behavior of the PD phenomenon is due to its unpredictable nature, and while some steps can be predicted statistically, accuracy cannot be assured. The amplitude, shape, and timing of PD pulses may be utilized to analyze PD phenomena while taking into account their stochastic nature. The occurrence of partial discharges in the power transformer's insulation system is determined most frequently by the presence of gas bubbles (from oil) or air pores left over from the impregnation process of the paper.

As a result, partial discharges degrade the dielectric characteristics of the insulation system, being caused by the current impulses generated into the cavities (or bubbles) by the partial discharges occurrence.

3.3 Thermal stress

If the power supply needs to grow, the increase in the transformer's load is translated (besides the electrical load and partial discharge growth) by the increase in its operating temperature (Fig. 3.2). Thus, high temperatures cause the acceleration of chemical reactions in the transformer's insulation system, leading to the important degradation of paper and mineral oil.

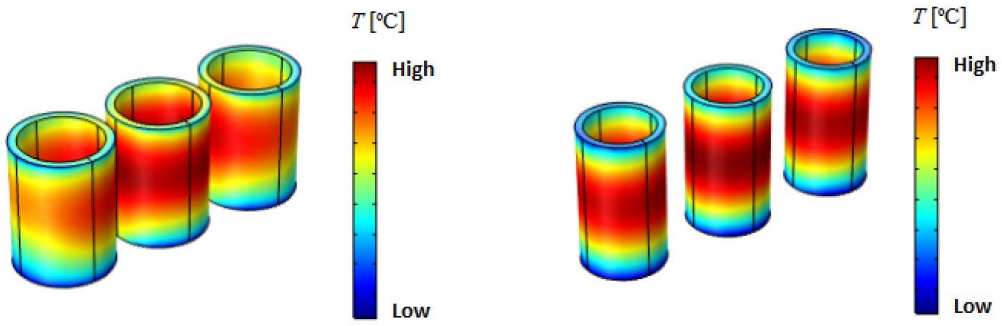

a) b)

Fig. 3.2. Temperature distribution during overload condition: (a) high voltage winding and (b) low voltage winding. [3.6]

Table 3.1. Maximum temperature limit for each operating regime. [3.7]

	Normal-function heating	Planned heating above the nominal limit	Long-term emergency charging	Thermal shocks
θ_{hs} at the level of windings (°C)	120	130	140	180
θ_{hs} for other metal components (in contact or not with the windings) (°C)	140	150	160	200
θ_{hs} oil (°C)	105	110	110	110

It should be pointed out that thermal stresses are regarded as the most hazardous (and the most frequently occurring) during transformer operation. The loading regimes of the transformer during operation determine the intensity and duration of the thermal stress, thus existing in the literature as a maximum limit of the *hot spot* θ_{hs} temperature (at the level of the windings and metal parts) and the oil temperature, as can be seen in Table 3.1. [3.7]

3.4 Mechanical stresses

The mechanical forces produced by the electromagnetic field on the conductive components are primarily responsible for the mechanical stresses in high-power electrical equipment. Additionally, the vibrations that also result from these electromagnetic forces cause the insulation in the transformer winding to continuously and significantly deteriorate. Also, the insulation on conductive components strips off as a result of temperature changes alternating expansions and contractions (that correspond to the different working regimes of transformers), and rubbing repeatedly wears down surfaces. From these perspectives, the mechanical efforts between the coil turns, between the coils, or between the distances, as well as the winding consolidation wedges, must be considered when designing and selecting the solid insulation.

As a result, the solid insulation (of the power transformers) must take over and resist all of the stresses and forces created by the electromagnetic field during normal operation, as well as short-term stressors caused mostly by accidentally short circuits. [3.1]

3.5 Environmental stresses

Analyzing the requests coming from the environment, we distinguish between natural stresses (referring to moisture, oxygen, etc.) and non-natural ones (see internal physicochemical reactions) [3.11].

The most important environmental factors are:

Oxygen: stands out as the most important degradation factor, causing the alteration of all insulation systems, whether solid or liquid.

Atmospheric humidity: damages the dielectric properties of the insulation, penetrating its composition. (Paper-oil insulation) [3.1]

Pollution and radiation: Besides industrial air pollution, solar radiation causes the power transformer temperature to grow. [3.8]

3.6 Transformer oil aging - mechanism

Regardless of the source, transformer oil chemical makeup is a mixture of more than 3000 organic elements, resulting in a wide range of chemical reactants and reactions as a consequence of the combined temperature and electrical activities that occur during electric equipment operation [3.9].

It is nearly impossible to set up a method for estimating the kinetic variables of the chemical mechanisms driving the degradation of the oil's physical qualities since all of these reactions produce products that considerably alter the oil's physical properties. Nevertheless, it should be noted that a variety of internal power transformer components (where energy losses originate and intensify) might influence the occurrence of this chemical reaction. High temperatures and electric fields, which can have high intensities in particular places as a result of the existence of some micro-defects or impurities, are the two most significant of these.

For the oil-paper insulation system, thermal stress is frequently viewed as the most significant change generator of the physicochemical characteristics [3.10]. Although the oil-paper insulation's thermal aging process is well understood, there are still questions surrounding the impact of high-strength electrical fields on the insulation system's component parts.

Additionally, under some circumstances, these combined heat and electrical stresses causes gas bubbles to emerge in the oil, which, in turn, causes partial discharges (PDs) to occur. [3.11] Recent research has shown that breaking hydrocarbon chains that appear in oil produces colloidal suspensions and soluble gases.

These by-products accelerate the oxidation of the transformer oil and are detrimental to the functioning of power transformers (PTs). The formation of soluble oxidation products along with insoluble sludge (that blocks heat dissipation owing to adhesion at solid insulation (cellulose)) is likewise promoted as a result of the chemical aggression of oxygen. Therefore, the creation of breakdown products is avoided if the chemical bonds of the molecular chains are stable. We list the heat energy (produced by the transformer's active components), the strong electric field (which starts the injection of electrons into the oil), and the dissolved oxygen as potential energy sources that might disrupt covalent bonds. [3.12] Furthermore, the partial discharges themselves represent a local source of radiation and heat (at a tiny scale, of course) emitted by ionized gas molecules (from bubbles), along with the continuous thermal stress brought on by radiating heat in the active components of the power transformer. Because all of these conditions coexist when partial discharges (during power transformer operation) happen, it follows logically that the effects of thermal stress cannot be openly delineated from those brought on by high electric fields and electromagnetic radiation.

CHAPTER 4

DIAGNOSTIC METHODS OF INSULATION SYSTEMS

This chapter discusses and describes widely used diagnostic techniques, including electrical, chemical, thermal and acoustic methods, with particular emphasis on electrical methods. The advantages of the electrical approach are highlighted, with emphasis on the analysis of dielectric response in the time and frequency domain, all to specifically fulfill the purpose of the study.

4.1 General consideration

The insulation system is largely responsible for most of the transformer's issues [4.1], emphasizing the importance of monitoring and diagnosing its insulation systems. Therefore, in this study, an accelerated aging approach for mineral transformer oil (a key component of PT insulation systems) by evaluating the main physical-chemical changes in its structure resulting from the action of a high-strength electric field and partial discharges is proposed.

4.2 Electric diagnosis methods

4.2.1 Time and frequency dielectric response analysis

Positive and negative charges are present in the microscopic structure of insulating materials, neutralizing each other at the macroscopic level. On the other hand, under the action of the electric field in an electrically insulating material, there is an orderly displacement of free electric charges, which means the phenomenon of electric conduction, but also a displacement of the related charges, i.e., the phenomenon of electric polarization of the material.

In this case, the material acquires an electrical moment of not null and also an electrical polarization of not zero. In addition to these two phenomena, there is also a movement of the electric charge between the insulation defects. As will be shown further, all these phenomena are closely related to the physicochemical structure of the insulation and the degree of its degradation, as reflected by the existence of free charge carriers and polar free radicals resulting from some electrochemical phenomena.

4.2.1.1 Time domain dielectric response analysis - absorption and resorption currents

A current $i_a(t)$ passes through the dielectric when a capacitor is subjected to a DC voltage step $U_0(t) = U_0\delta(t)$ for a time of T_c (Fig. 4.1).

$$i_a(t) = i_{ch}(t) + i_p(t) + i_{s\_ch}(t) + i_c(t) \tag{4.1}$$

δ(t) represents the step delta variable. [4.1]

$$\delta(t) = \begin{cases} 0, & \text{if} \quad t_0 > t > T_C \\ 1, & \text{if} \quad t_0 \leq t \ \leq T_C \end{cases} \tag{4.2}$$

where $i_a(t)$ is the absorption current, $i_c(t)$ is the conduction current that describes the capacitor dielectric's conductivity for the direct current σ_{DC}, $i_p(t)$ is the current of polarization, $i_{s\_ch}(t)$ is the current of space charge and $i_{ch}(t)$ is the amount of current required to charge a capacitor with air acting as the dielectric. [4.2]. The current $i_{ch}(t)$ equates the capacitor that has vacuum as dielectric and rapidly declines to zero, so this is why it is not recorded in the majority of experiments. The polarization current $i_p(t)$ relates to dielectric polarization occurrences that include low spatial motions of bounded charges and gradually drop to zero.

The current $i_{s\_ch}(t)$ relates to the space charge in the insulating quantity (oil), which is mostly caused by the deterioration process and charge injection phenomena (owing to shape imperfection, for example). Also, $i_{s\_ch}(t)$ gradually declines to zero.

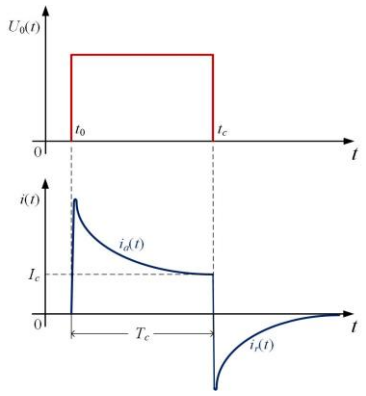

Fig. 4.1. Absorption $i_a(t)$ and resorption $i_r(t)$ current time variation. [4.1]

Convection of free charge carriers like ions, electrons, and so on generates the conduction current $i_c(t)$. Also, the physical structure and chemistry of the capacitor's dielectric are the main factors that affect any charge carrier's species concentration [4.1]. The electrical conductivity or resistivity of the dielectric (aged mineral oil in our case) may be estimated using this current component.

The resorption current $i_r(t)$ can be obtained by short-circuiting the capacitor electrodes at time $t = T_c$ and by ceasing the voltage application:

$$i_r(t) = i_d(t) + i_{dp}(t) + i'_{s\_ch}(t), \tag{4.3}$$

where the vacuum dielectric capacitor's discharge current is denoted by the symbol $i_d(t)$, the depolarization current by the symbol $i_{dp}(t)$, and the dielectric space charge current by the term $i'_{s\_ch}(t)$.

When the voltage that is being used is small (e.g., below 1 kV) and the applied time is of the order of a few minutes or hours (which implies no significant decomposition of chemicals; there is no variation in the number of charge carriers and polar dipole concentration), the polarization and depolarization currents and space charge currents are quite the same ($i_{s\_ch}(t) \cong i_{s\_ch}'(t)$ and $i_p(t) \cong i_{dp}(t)$), and the conduction current can be estimated as [4.2]:

$$i_c(t) = i_a(t) - i_r(t) \tag{4.4}$$

4.2.1.2 Frequency domain analysis of the dielectric response

Dielectric spectroscopy (in the frequency domain) investigates the interaction of an electromagnetic field with a dielectric material over a large frequency spectrum ranging from 10^{-6} to 10^{12} Hz [4.3]. This is an extremely efficient method for studying the structure and dynamics of insulation systems, assessing the phenomena of conduction and slow polarization (e.g., orientation and interfacial; see Fig. 4.2) that occur at significantly lower frequencies compared to the phenomenon of quick polarization (e.g., electronics and ionic) [4.1, 4.4].

In line with the purpose of this PhD thesis, the dielectric spectroscopy was utilized for evaluating the behavior of unaged and accelerated-aged oil.

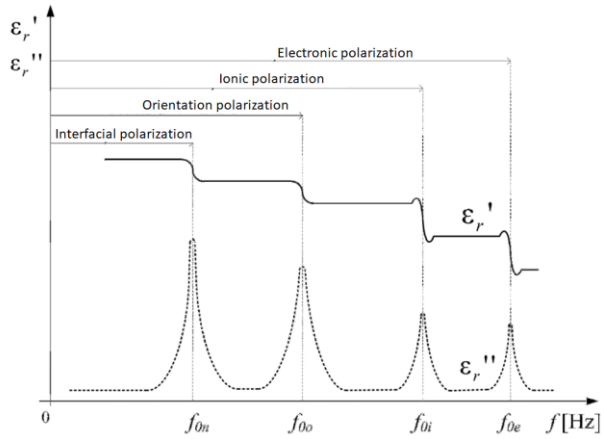

Fig. 4.2 Variation of complex permittivity components (ε_r' and ε_r'') function of electric field frequency. [4.4]

Quantities that best represent the conduction and polarization mechanisms in the frequency range are relative complex permittivity, and conductivity. That may be obtained by applying a time-varying electric field (of value 1 *VAC*) to a dielectric material (mineral oil in the case of this study). The characteristic measurement method of dielectric spectroscopy consists of determining the dielectric properties of the tested material as a function of the frequency of the electric field exerted on it.

Thus, in a measuring cell that houses a planar test sample of thickness *d* bordered by two electrodes that describe an area *A*, a planar capacitor is formed. If a sinusoidal voltage U_0 of frequency $f = \frac{\omega}{2\pi}$ (where ω is the pulsation [4.5]) is applied to this capacitor, a current I_0 of the same frequency is generated, but with angle φ phase-shifted before the voltage. **Electrical conductivity and relative permittivity**, as well as the sample's form (electrode area and electrode spacing or sample thickness), define the relationships between voltage, current intensity, and the phase difference between them.

4.3 Power transformer insulation system chemical diagnosis methods

4.3.1 Dissolved gas analysis

Dissolved Gas Analysis (DGA) has been identified as an essential approach for detecting incipient defects in power transformer (PT) insulation. It evaluates the PT condition by measuring the concentration of different gases dissolved in transformer oil that emerge during operation due to thermal and electrical stressors. The decomposition of paper and oil produces vapors that, when dissolved in transformer oil, impair its dielectric strength. Among the gases dissolved in transformer oil are combustible gases such as hydrogen, carbon monoxide, methane, ethane, ethylene, acetylene, and noncombustible gases such as carbon dioxide, nitrogen, and oxygen.
Overheating, partial discharges, and continuous arcing create a wide spectrum of gases, and their concentrations that will enable us to determine the severity and origin of the faults.

Many techniques have been developed for interpreting DGA data, including: the key gas, Doernenburg ratio, Rogers ratio, IEC ratio, and Duval triangle methods. [4.6]

4.4 Thermal and acoustic methods for transformer insulation diagnosis

4.4.1 Infrared thermography

Temperature increases over nominal levels as a result of problems with transformer cooling (such as radiators, pumps, etc.) as well as from losses in the magnetic core or the windings. Infrared thermography is used to remotely identify thermal deviations. This monitors the infrared radiation released and converts it into an electrical signal, making it possible to locate obstructions in the cooling system, hot areas, poor electrical connections, etc. [4.1]

4.4.2 Fault detection by ultrasound

This test is capable of detecting both continuous discharges (electric arc) and partial discharges (corona) caused by transformer operation. Because partial discharges indicate the local breakdown of the insulating environment, they cause charge redistribution within the insulation system, resulting in 'noise'. Sonic tests examine the increase in noise and vibrations caused by various parts (such as the magnetic core, coils, and so on). [4.1]

CHAPTER 5

AGING CELL SETUP AND EXPRIMENTAL METHOD

This chapter details the characteristics of the aging cell, including its geometric layout with the metallic electrode. It also discusses the mathematical model for computation, material properties, and numerical models for three- and six-disc metallic electrodes. The final configuration and design of the aging cell are established, along with process steps for method preparation. The study has chosen the six-disk electrode for laboratory testing of accelerated oil aging based on numerical calculations and experimental findings. The results highlight electrical discharging, bubbling, and color change in the oil, ensuring that the study's objectives are met.

5.1 General consideration

Partial discharges, caused by high-strength electric fields, are local sources of heat on a small scale. Although the thermal stress process of transformer oil is recognized as the most important element affecting its physicochemical characteristics [5.1], there is still ambiguity regarding the impact of the high electric field on oil components

However, there are few studies on the changes in dielectric characteristics of oil under high-strength electrical fields and partial discharges. Thus, an innovative method for accelerating the aging of mineral oil by applying an intense electric field and partial discharges was developed for laboratory use.

The ASTM D 6180-05 [5.2] standard analyzes the impact of the high strength electric fields and partial discharges on oil characteristics, focusing on the effects of strongly ionized gases generated by electric field at the oil surface, not of partial discharges in the oil volume. The study aims to accelerate aging oil by creating a local high electric field in the oil volume, resulting in PDs. To achieve this, two electrode types were designed to determine the most efficient method for developing and forming gas bubbles in the oil volume.

5.2 Aging cell design

The aging cell design concept entails using a dielectric barrier (glass) that is very stable thermally, chemically, and under stress caused by the high-strength electrical field and PDs. In terms of the characteristics of the inner metal electrode, it is emphasized that it must have rounded corners and no sharp edges to prevent charge injection. Additionally, the inner metallic electrodes (for both variants) were developed to assist in the creation of gas bubbles and the formation of gas bags, which in turn will facilitate local electrical discharges. [5.3]

5.2.1 Geometrical models

The whole model was set up on suppling availability, and a test tube (dimensions of 130 mm high, 14 mm inside diameter, and 1.25 mm thick walls) composed of glass that is both dielectrically and thermally stable was selected [5.3]. By serving as a dielectric barrier between the outer electrode, composed of a salt water solution, and the inner metallic electrode, this tube prevents the oil in the inter-electrode gap from completely dielectrically breaking down.

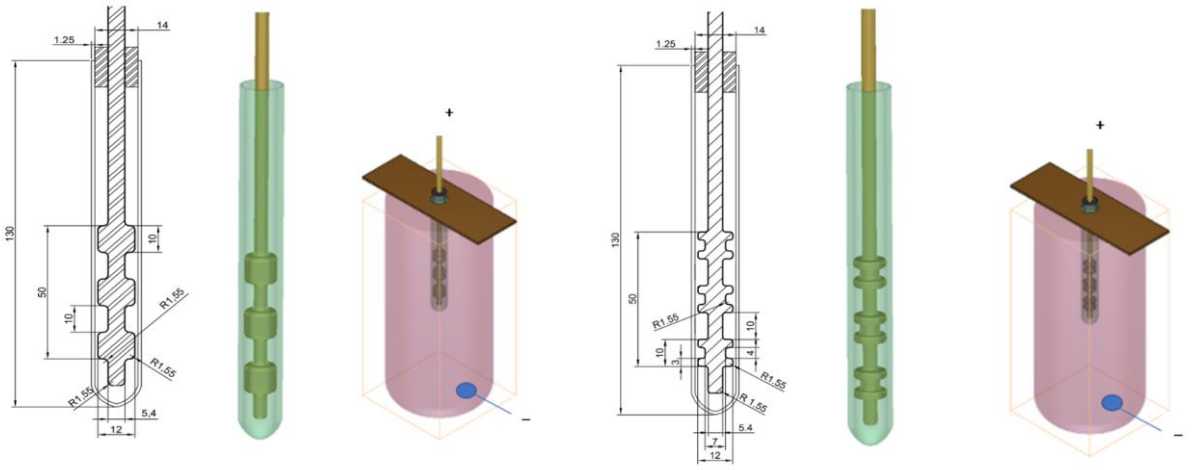

a) b)

Fig. 5.1. Metallic electrode geometry and aging cell concept a) three discs; b) six discs.

Inside the glass tube, a metallic electrode was foreseen to be introduced, consisting of a cylindrical rod having rings (discs) with an external diameter of 12 mm.

The electrode surface and the ray margins received particular attention to meet both the concept detail requirements and the execution and replication limits.

For the initial simulation, two design types with three and six disks were chosen for the metallic electrode, which was thought to be made of brass (see Fig. 5.1). The electrode geometry seeks to generate a high-intensity electric field and bubbles into the oil volume, which will subsequently trigger partial discharges.

The oil gap between electrode discs and glass wall was set up at 1 mm, looking to evaluate (by computation firstly, using COMSOL Multiphysics) the intensity of the electric field, knowing also that the dielectric strength of transformer mineral oil is greater than 15 kV/mm.

The second (outer) electrode was designed to be produced by immersing the aging cell in an electrically conductive solution (a water-sodium chloride mixture).

As shown in Fig. 5.1, a stainless-steel electrode is immersed in salt water, and the voltage is applied and controlled, between the metallic electrode and the salt solution (i.e., the ground stainless-steel electrode).

5.2.2 Numerical computation of electrical condition in the aging cell (electric field computation)

5.2.2.1 Physical model

The physical model is shown in Fig. 5.1. Sizing the aging cell based on the electric field distribution involves determining the electric field values in the space between the inner metal electrode and the outer electrode connected to zero potential. Therefore, the electric field distribution in the oil and glass walls (of the aging cell) will be computed, considering all linear, homogeneous, and isotropic media.

5.2.2.2 Domain of calculation

5.2.2.3 Mathematical model

5.2.2.4 Border conditions

5.2.2.5 Simulation results – metallic electrode with six discs

For greater precision in the area where the electric field intensity is higher, a much finer discretization network was chosen than in the rest of the calculation domain. After the mesh was created, the distribution of the electric potential and the electric field was calculated and presented in Fig. 5.2 for the six discs electrode type (Fig.5.1b). The electric field streamlines are concentrated (intense) on the radius and edges of the electrode shape. Streamline indicates the concentration of the electric field in the edge areas of the electrode (in the geometric radius), thus indicating that the phenomenon of molecular dissociation of the oil with subsequent formation of gas bubbles and initiation of partial discharges (PD) (due to the lower relative permittivity of the generated gases) will be a phenomenon that depends on the geometric shape of the electrode.

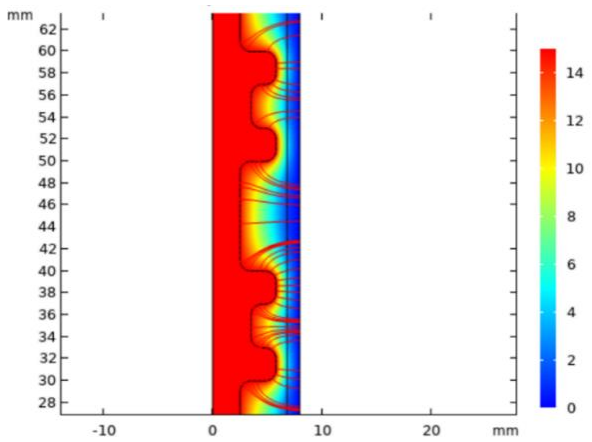

Fig. 5.2. Electric Field streamlines.

The phenomena simulated or explained above were monitored by practical experiments performed in the laboratory (e.g., intense gas bubbles and PDs between electrode discs).

5.2.2.5.1 Electric field distribution for six disc electrode design

From a broader perspective, the values of electric potential and electric field strength (ex. Fig. 5.4 and Fig 5.5) in the oil volume were analyzed at different points and directions of computation.

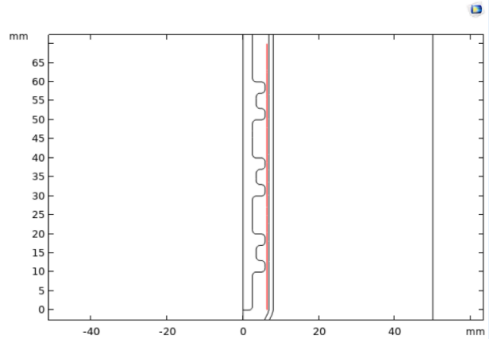

Fig. 5.3. Axial direction in the oil volume used for electric field computation.

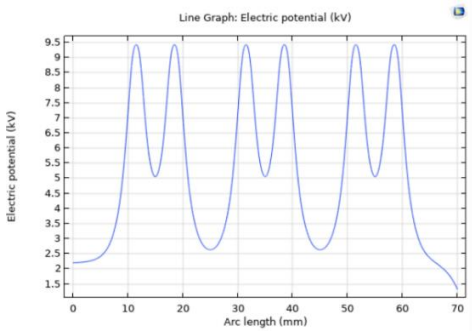

Fig. 5.4. Electric potential variation in the axial direction (in the oil volume).

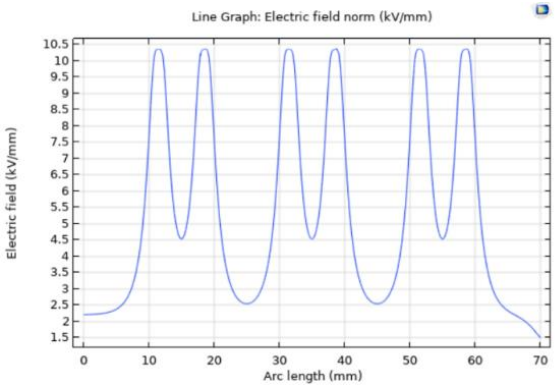

Fig. 5.5. Electric Field variation in the axial direction (in the oil volume).

Thus, in the axial direction (Fig. 5.3), it can be seen that the electric field value is in the range of intensity ~10.5 kV/mm, enough to foreshadow the generation of electric discharges in the oil volume and also adequate to avoid total electric breakdown of the oil gap between the electrodes (knowing that the dielectric strength of transformer mineral oil is higher than 15 kV/mm). These results allow us to initiate practical laboratory tests for accelerating the aging of the mineral oil under the action of the high-strength electric field and the partial discharges.

5.2.2.6 Simulation results – metallic electrode with three discs

The electric potential, electric field distribution, and their intensity values were calculated theoretically for the electrode composed of three discs (see Fig. 5.1a). The steps followed were the same as those from the six-disc electrode simulation: making the mesh and applying the electric potential value of 15 kV to the electrode from the aging cell. The gap between the electrode disc and the inner glass test tube remains 1 mm, identical to the previous simulation of the electrode with six discs.

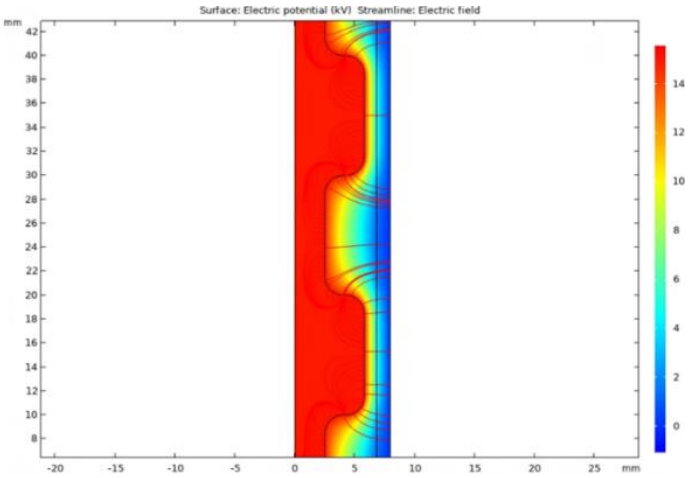

Fig. 5.6. Electric Field streamlines (three discs electrode).

The same observation regarding the electrical potential value (applied to the brass electrode), that decreases toward the glass tube wall where the boundary condition of electric potential $V = 0$ is imposed. Also, the electric field streamlines are concentrated in the electrode's radius areas (edges) as shown in Fig. 5.6.

An additional remark is reveled for the electric field streamline distribution with regards to the fewer numbers of the edges (i.e., number of discs), which derives from lower areas of electric field concentration, resulting in a potentially mild aging intensity (fewer bubbles and PDs). This behavior will be monitored and evaluated in laboratory experiments, thus assessing aging intensity.

5.2.2.6.1 Electric field distribution for three disc electrode design

The electrical field values and electric potential distribution in the oil volume, was also assessed for the three-disc electrode model (Figs. 5.7,5.8 and 5.9). Firstly, a distinct pattern variation (due to the metallic electrode design) was observed with peak values that were lower than in the case of the six-disc electrode. Thus, this result in the electric field top value in the domain range of 10 kV/mm (Fig. 5.9), which is slightly lower (~0.5 kV/mm) than the values found for the six-disc electrode (Fig. 5.5).

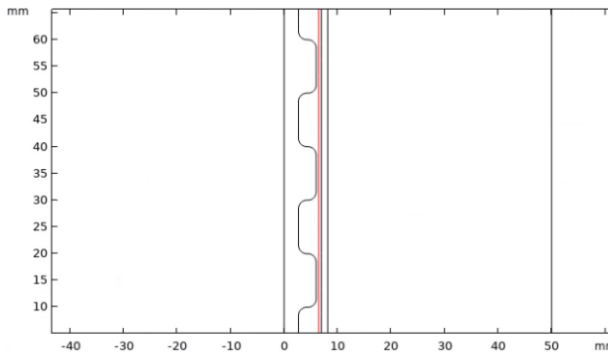

Fig. 5.7. Axial direction in the oil volume used for electric field computation (in the oil volume).

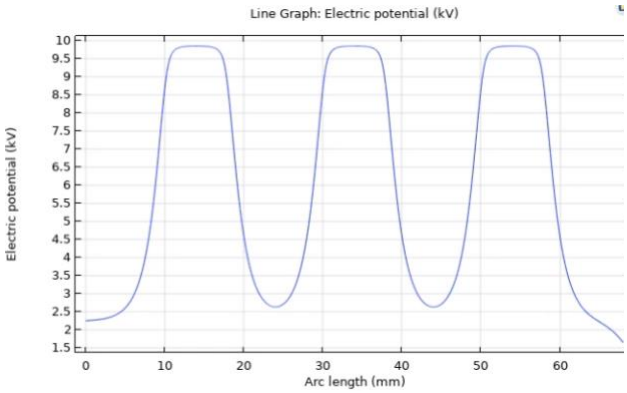

Fig. 5.8. Electric potential variation in the axial direction (in the oil volume).

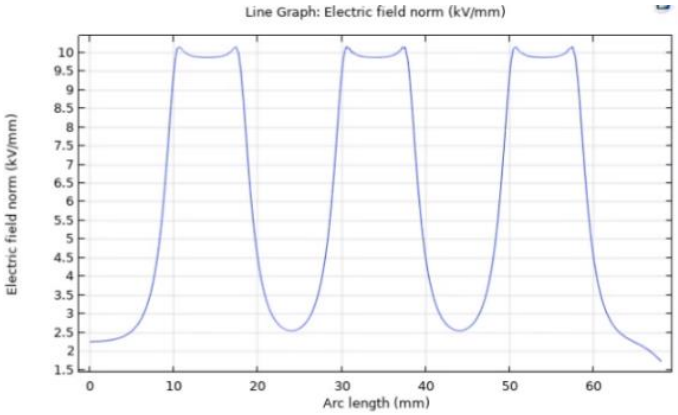

Fig. 5.9. Electric Field Strength (in the oil volume).

The peak values of the electric field intensity at the extremities of the disc areas are owing to the radius of the disc that focuses and concentrates the electric field.

Final observation is related the attenuation of the electric field strength value and its dispersion in the case of the three-disc electrode (relative to the six-disc electrode COMSOL simulation), all of them being primarily driven by the electrode geometry. Even though the modeling result suggests that the six-disc electrode has more aging efficiency, both designs in a lab experiment were evaluated, obtaining the results that will be shown in the paragraph that follows.

5.3 Experimental analysis

The two electrodes (see Fig. 5.1 a and b) were made within the limits of practical possibility in order to achieve a duplication of their fabrication and, consequently, to ensure repeatability (for test consistency) of the intense electric field conditions in the aged cells. Some remarks were raised after testing the two electrode types, the most important being related to the amount of gas bubble, which is significantly bigger for the electrode with six discs. Therefore, although the aging process initiates and develops in the same manner (specifically, the gas bubbles emerge at the free surface of the oil and progress to take up the entire oil volume), the electrode with six discs exhibits a more severe aging process compared to the three-disc electrode throughout a similar aging period (see Fig. 5.10). The severity of the aging process may be readily assessed by visual inspection of the oil color, which is more pronounced for the six-disc electrode. Given these considerations, the electrode with six discs was employed in the subsequent research.

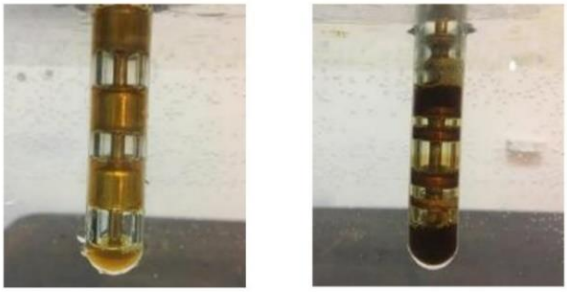

Fig. 5.10. Oil aged for 8 hours: a) three discs; b) six discs.

5.4 Methodology

The aging method seeks to limit the influence of external factors on the oil throughout the aging process. Thus, the preparation of the cell prior to the start of the aging process consists of sealing the oil with nitrogen-inert gas (once the test tube has been filled with oil) at its open surface and utilizing a special plug that centers the electrode's position in the test tube, sealing both the oil and nitrogen. Given the fact that high pressure occurs in the cell throughout the experiment, gas bubble development results exclusively from the reactions that happen within the oil quantity under the action of an intense electric field (same as the power transformer operation, reminding us that the transformer is hermetically sealed) without the involvement of other atmospheric gases (i.e., oxygen, etc.).

Additional focus has been given to electrode surface polishing as a way to prevent local punctual electrical field concentration and to guarantee consistency of the findings throughout all aging cells.

5.4.1 Final aging cell design

A key characteristic of the cell is the test tube made of a unique glass (extremely stable thermally and dielectrically) having an interior diameter of 14 mm and a height of 130 mm that can host an oil volume of 8 ml. The brass electrode is positioned inside the glass tube and consists of a cylindrical rod with six discs, having an outside diameter of 12 mm; hence, there is a 1 mm gap between the disks and the glass wall. A high electrical field is generated by immersing the cell in a solution of salt water (strong conductivity) connected to the ground and by supplying a high voltage (0 - 50kV and f = 50Hz) to the brass electrode.

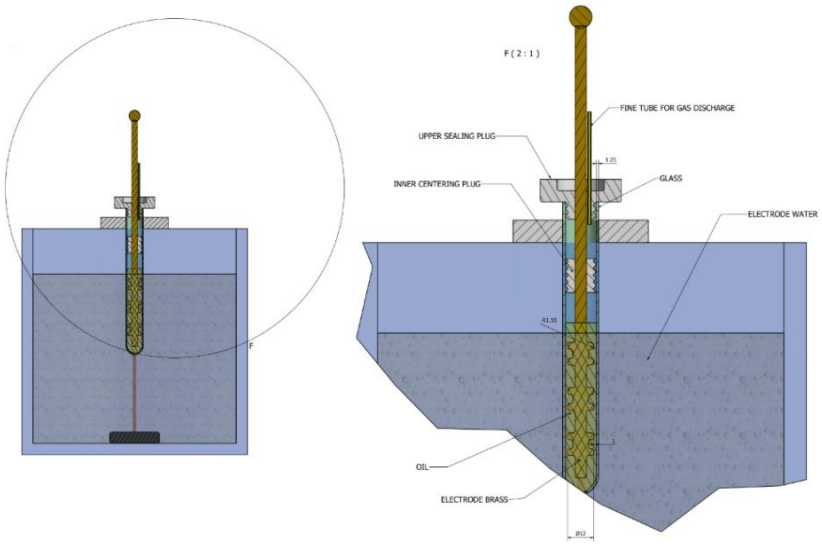

Fig. 5.11. Design and setup of aging cells.

The thickness of the test tube glass wall is 1.25 mm, as shown in Fig. 5.11 and the brass electrode has rounded edges with a 1.55 mm radius, avoiding any defects (or imperfections) and sharp edges that might induce charge injection or focused local electric field concentration. A noteworthy characteristic that needs to be mentioned is the tiny hole in the upper plug, which aims to evacuate the gasses generated inside the cell during the aging process and is necessary to prevent overpressure inside the glass tube. The second electrode is a water-based solution containing sodium chloride that is placed externally of the cell, surrounding it and offering excellent contact with the cell glass tube. The voltage is applied in this way between the inner brass electrode and a metal (stainless steel) electrode submerged in salt water.

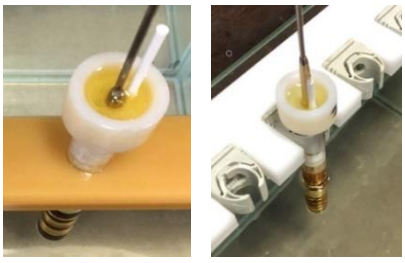

Fig. 5.12. Aging cell outer plug.

There is an important correlation between the volume and initial level of oil within the cell since it should be around 15 mm underneath the inner plug because of the bubble formation phenomenon that results in a rise in the oil level in the cell. In this way, a specific volume is ensured, considering that this volume was initially filled with nitrogen gas.
Concerning the oil expansion phenomenon, the upper plug is built in such a way that it collects oil leaks throughout the aging process. These gaseous products and oil vapor discharges (which come up from cell overpressure) are pushed through the small tube, as shown in Fig. 5.12.

5.4.2 Experimental setup

The accelerated electrical aging experimental setup comprises a glass tank containing salt water into which the aging cells are partially submerged, as shown in Fig. 5.13. The aging cell support can accommodate up to 5 cells that can be powered simultaneously by applying an electrical voltage between the inner metallic electrode (brass) and the saltwater solution with a stainless-steel electrode submerged. Thus, the voltage can be changed from 0 to 50 kV, and the aging cells are video recorded by a camera that captures up to 30 frames per second throughout the aging process. The timer is used to time the application of voltage, and the current relay, which is attached to the low-voltage section of the transformer, is intended to cut off power in the event that an aging cell's glass tube breaks accidentally. The aging tests were conducted using MOL mineral oil samples designed and intended specifically for use in power transformer insulation systems.

Oil was treated for 72 hours at 60 degrees Celsius in a forced-flow oven before being placed in the aging cell. Several process steps as part of the aging cell preparation technique were established. Thus, prior to doing anything else, a thorough cleaning of all the cell parts with alcohol was done, blowing compressed air over them, and then drying them in a heated oven at 50 ^{0}C for a minimum of 15 minutes. Mineral oil in an 8 ml amount was carefully added to the test tube without allowing air bubbles to emerge. Then, to isolate the oil from interaction with ambient air, nitrogen gas was released above the oil at its open surface. The brass electrode and its inner and outer plugs were then successively inserted into the cell, adjusting and holding the electrode in the proper position. Lastly, the finished cells were heated to 50 ^{0}C for 15 minutes in the oven. All tests were conducted in the laboratory at ambient temperature, with an electric potential gradually applied to the brass electrodes till it reached a value of 16 kV, at which stage the bubble formation phenomenon started and subsequently partial discharges occurred.
After the electrical discharges have propagated throughout the oil volume, the voltage value has been slightly lowered to 13 kV. It has been confirmed that during the aging test, gas bubbles and partial discharges manifest themselves at this voltage level during the whole process.

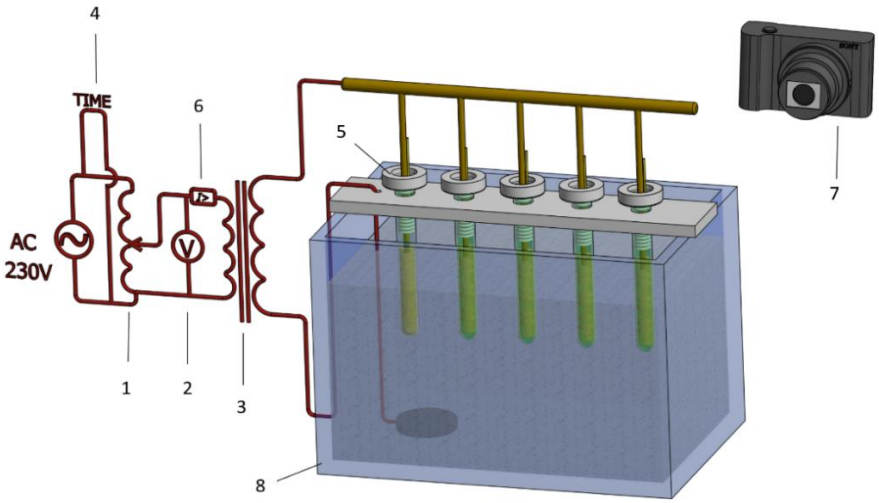

Fig. 5.13. Experimental approach: 1–adjustable transformer used for set-up the voltage value; 2–voltmeter; 3–high voltage transformer; 4–timer; 5–aging cell; 6–current relay; 7–camera with video recorder and 8–glass tank.

The experiments were carried out on a minimum of three samples for each aging time. To ensure consistency of results, the final results were an average of the three measured values.

5.4.3 Visual experimental findings

Regarding the various aging phases, a few observations were made. Firstly, the gas bubble formation phenomenon is obvious and easy to detect, initiating from the oil free surface and extending into the entire oil amount (Fig. 5.14a). As the gas bubbles develop, small, dispersed, bright electrical discharges can easily be detected within the aging cell, as illustrated in Fig. 5.14b.

a) b)

Fig. 5.14. a) Bubbles gas inside the aging cell; b) Luminous electrical discharges within the bubbles.

An essential point to emphasize in the later phases of the aging process is the formation of gas bags between the inner brass electrode discs; thus, gas bubbles gather into bags, impacting the aging process dynamics. Moreover, even after the electrode voltage has been turned off, the gas bags formed during the aging process are maintained, sustained, and preserved. (See Fig. 5.15).

Fig. 5.15. Gas bags kept in aging cells.

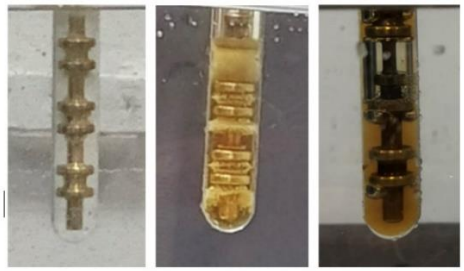

Fig.5.16. The color of the oil changes as it is aged: a) unaged oil; b) aged oil 3 hours; c) aged oil 8 hours.

Apart from analytic data, which will be described in depth in the next chapter, the stage of the aging process may be qualitatively indicated by a visual inspection of the oil color over the aging process. As illustrated in Fig. 5.16, if the color of virgin oil is almost completely colorless, the shade of the oil becomes darker as the length of the voltage application grows [5.4].

CHAPTER 6
INFLUENCE OF THE AGING PROCESS ON THE MINERAL OIL CONDITION

In this chapter, we discuss experimental results and methods used to assess oil characteristics. It provides an explanation of the spectroscopy dielectric approach and examines diagnostic factors (as well as complementary ones) used in oil characteristics assessment.

The study emphasizes complex conductivity to identify conduction processes in oil degradation stages. The hypothesis of generating charge carriers from different species, which are more mobile and easily activated, is explored to explain the significant rise in conductivity due to increased concentration of free charge carriers. The study determined the mean mobility of conduction ions and activation energy for different aging times and temperatures, confirming the hypothesis that hydrocarbon molecules fragment perpetual due to partial discharges and high-strength electric fields.

6.1 Introduction

Dielectric spectroscopy is a well-known technical method for analyzing the interaction between a material and a harmonic electric field exerted on it, providing information about molecular dynamics over a wide range of frequencies at different temperatures. The new dielectric instruments allow broadband dielectric spectroscopy (BDS) to be performed from ultra-low frequencies 10^{-6}Hz to infrared frequencies in the 10^{12}Hz range. [6.1, 6.2].

In recent times, dielectric spectroscopy has significantly advanced due to advancements in software and electro-technical advancements. This method, based on polarization and electrical conduction, is widely used for insulation system diagnosis and aging assessment.

6.2 Dielectric spectroscopy method

To assess the accelerated aging process of mineral oil under the influence of high-strength electric fields and partial discharges, the dielectric properties of the oil samples were measured using dielectric spectroscopy. For this purpose, a Novocontrol spectrometer (Fig. 6.1) and a special measuring cell for dielectric liquids with a volume of ~1.8 ml was utilized (Fig.6.2). The real and imaginary parts of the complex relative permittivity (ε_r' and ε_r''), dielectric loss factor tg δ and complex conductivity ($\underline{\sigma}$) were measured in a frequency range of $3 \cdot 10^{-3}$ to 10^3 Hz.

Fig. 6.1. Dielectric Spectrometer 1 – PC; 2 – Central unit; 3– Measuring cell; 4 – NovoTherm temperature control system; 5 – Command unit;

Fig. 6.2. Oil measuring cell;

Samples of aged oil were added one at a time to the liquid measuring cell of the spectrometer to determine how the dielectric properties of the oil were affected by the aging process. The effect on the dielectric properties of mineral oil samples was evaluated for a frequency range between 3 mHz and 1 MHz at different temperature levels. The measurements were executed utilizing a dielectric spectrometer, and all oil samples before being tested were kept in the oven for 12 hours at 50°C (using a 10 ml bottle) with the goal of physicochemical stabilization. Recall that for result consistency, each experimental value was calculated as the average of three measured results.

Regarding the method of the measurement process, a voltage $u(t)=U_{RMS}\sqrt{2}\cdot\sin(\omega t)$ of known frequency f shall be considered being applied through the measurement cell electrodes to the test sample. Thus, the spectrometer will measure a current $i(t)=I_{RMS}\sqrt{2}\cdot\sin(\omega t-\varphi)$ which has a phase shift φ with respect to the applied voltage, the RMS index specifying the mean square value of $u(t)$ and $i(t)$ and the pulsation has the form $\omega = 2\pi f$. Therefore, the result provided by the spectrometer will be an impedance $\underline{Z}$ associated with the test sample (accelerated aged oil in our case). The tested oil sample has complex capacity $\underline{C}$ of the following relation form:

$$\underline{C} = \frac{1}{j\omega \underline{Z}(\omega)} = \underline{\varepsilon_r} \cdot C_0 = [\varepsilon_r'(\omega) - j\varepsilon_r''(\omega)]C_0, \quad (6.1)$$

where ε_r'(ω) and ε_r''(ω) mean the real and imaginary parts of the complex relative permittivity of the oil sample, C_0 represents the empty cell capacity, and $j^2 = -1$. [6.3]

Moreover, the dielectric loss factor can be calculated accordingly with the following relationship [6.4]

$$\operatorname{tg}\delta = \frac{\varepsilon_r''}{\varepsilon_r'} \quad (6.2)$$

Furthermore, the spectrometer will measure the complex conductivity of the test sample, which will be calculated as the ratio from (6.3) relation, i.e., the proportion between the relative complex permittivity and the impedance of the empty measuring cell Z_0:

$$\underline{\sigma} = \frac{\underline{\varepsilon_r}}{Z_0(\omega)} = j\omega\varepsilon_0\underline{\varepsilon_r} = \omega\varepsilon_0\varepsilon_r''(\omega) + j \cdot \omega\varepsilon_0\varepsilon_r'(\omega) \quad (6.3)$$

where, $\sigma'(\omega) = \omega\varepsilon_0\varepsilon_r''(\omega)$ is the real parts of complex conductivity and $\sigma''(\omega) = \omega\varepsilon_0\varepsilon_r'(\omega)$define imaginary parts of complex conductivity. [6.3]

If the frequency of the applied voltage has a low value, σ' can be approximated by the value of the σ_{DC} ($\sigma' \cong \sigma_{DC}$) meaning static conductivity. Thus, examining the low-frequency areas where the real conductivity spectrum σ' is constant, the static conductivity of the mineral oil samples is identified. Conversely, we have the Jonscher relationship, which illustrate increases in the real part of the complex conductivity for higher frequencies [6.5, 6.6]:

$$\sigma'(\omega) = \sigma_0 + A(T)\omega^n = \sigma_0[1 + (\omega \cdot \tau)^n], \quad (6.4)$$

thus, for a reduced frequency, the value of $\sigma'(\omega) \cong \sigma_0 \cong \sigma_{DC}$ is the static conductivity above discussed.

The last part of the Jonscher equation $A(T)\cdot\omega^n$ represents σ_{AC}; the frequency-dependent term, known as the dissipative part of conductivity (having exponent $n \cong 1$ for mineral oil), and characterizes the motion of the charge carriers (ions) over short distances. Equation (6.4) contains relaxation time τ corresponding to the electric relaxation phenomenon, which models and makes $\sigma'(\omega)$ a powerful law characterized by n ($0 < n \leq 1$), when $\omega\cdot\tau >> 1$, and also makes $\sigma'(\omega) \cong \sigma_0 \cong \sigma_{DC}$ when $\omega\cdot\tau << 1$. [6.3]

The electrical relaxation phenomenon mentioned above is explained in more detail in [6.1, 6.7], being related to the mobility of the free ions in structurally disordered dielectric media, such as mineral oils produced from various combinations of hydrocarbons.

6.3 Experimental results and discussion

Variations with frequency and temperature for the main diagnostic factors of accelerated electrically aged MOL mineral oil will be presented in the following paragraphs, highlighting and insisting on the particular phenomena resulting from this process.

6.3.1 Complex relative permittivity and dielectric loss factor

Figs. 6.3, 6.4, show the real components of the complex relative permittivity with frequency at various aging durations for temperature range of 25 °C, 40 °C,; meanwhile, Figs. 6.5, 6.6, show the imaginary components of the complex relative permittivity with frequency at various aging durations and same temperatures . The findings presented, reveal that the changes in ε_r' and ε_r'' are typical for mineral oil in the case of unaged, conditioned oil, as quantified and displayed in some earlier investigations [6.8].

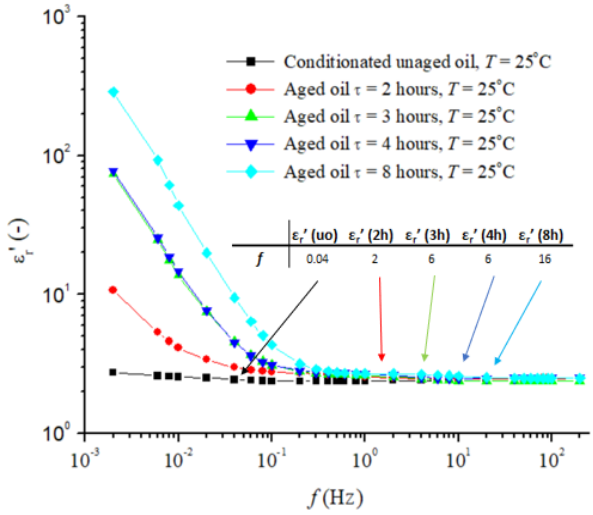

Fig. 6.3. Real part of the complex relative permittivity (ε_r') variation as a function of frequency for various aging times (measurement temperature T = 25 °C and aging applied voltage U = 13 kV).

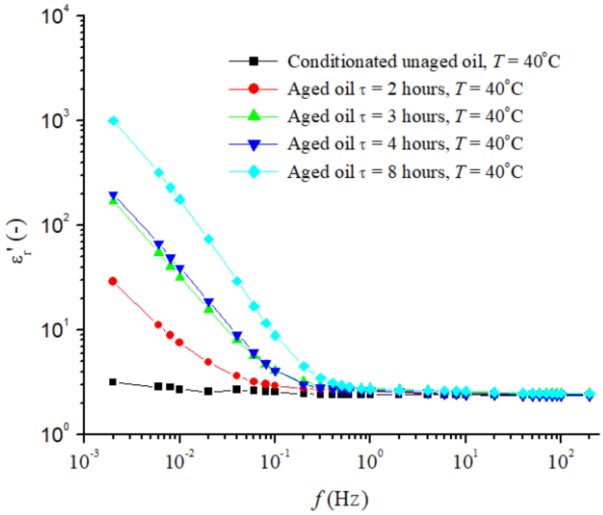

Fig. 6.4. Real part of the complex relative permittivity (ε_r') variation as a function of frequency for various aging times (measurement temperature T = 40 °C and aging applied voltage U = 13 kV).

Nevertheless, examining the samples that have been aged, the values of ε_r' significantly grow, particularly when the applied electric field frequency falls under 0.1 Hz. Also, the same situation is observed in the case of ε_r'', which, in a wide range of frequencies, takes much higher values compared to those of unaged oil (Fig. 6.5-6.6). Generally, this indicates a high concentration of polar free radicals and free charge carriers, which proves the existence of strong deterioration processes in the oil. These, of course, cause the electrical conduction and polarization processes to become more intense.

Special consideration must be given to the complex relative permittivity's variation with frequency, as in the low-frequency range, every molecule (implicitly the dipoles) could follow electric field variations. As a result, the real part of relative permittivity's value remains unchanged as frequency reduces, a phenomenon that is outlined by the plateau level (value) of $\varepsilon_r'(\omega)$ (see Figs. 6.3-6.4).

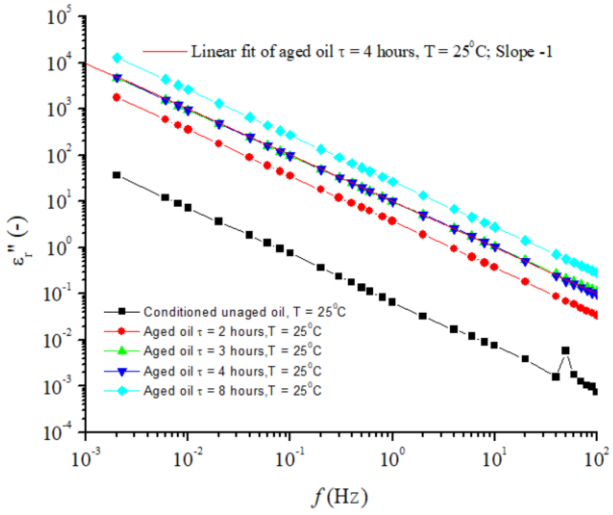

Fig. 6.5. Imaginary part of the complex relative permittivity (ε_r'') variation as a function of frequency for various aging times (measurement temperature T = 25 °C and aging applied voltage U = 13 kV).

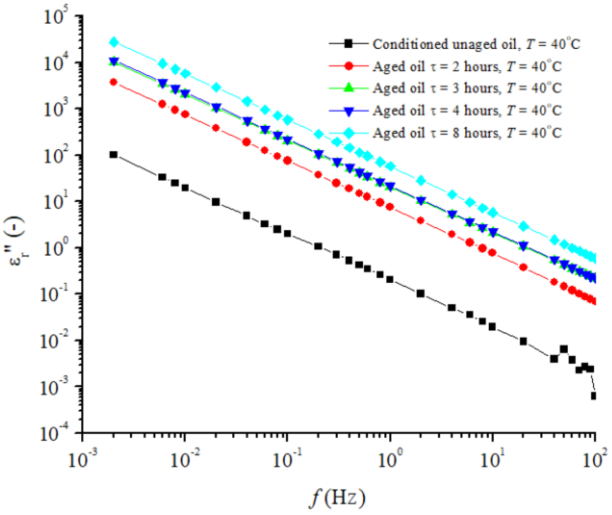

Fig.6.6. Imaginary part of the complex relative permittivity (ε_r'') variation as a function of frequency for various aging times (measurement temperature T = 40 °C and aging applied voltage U = 13 kV).

As already known, $\sigma'(\omega) = \omega\varepsilon_0\varepsilon_r''(\omega)$ and, if $\sigma'(\omega) = \sigma_{DC} = ct. \rightarrow \varepsilon_r''(\omega) = \frac{\sigma'(\omega)}{\omega\varepsilon_0}$ and as a consequence, the fluctuation of $\varepsilon_r''(\omega)$ is inversely correlated to ω (i.e., frequency), and the line on the graph representing the variation of $\log \varepsilon_r''$ with $\log \omega$ will have a slope of -1 (Fig.6.5). It represents an example of a basic conduction phenomenon where σ_{DC} may be estimated at a low frequency corresponding to the diagram area where we have a linearly variation with a slope of -1 for $\varepsilon_r''(\omega)$ and real part of complex relative permittivity $\varepsilon_r'(\omega) = ct.$ [6.9] It is worth paying close attention to how ε_r' and ε_r'' vary in very low frequency. Thus, an increase in the value of ε_r' once the frequency of the electric field drops may be explained, consistent with Debye theory [6.1], by the electrical relaxation processes that occur at low frequencies.

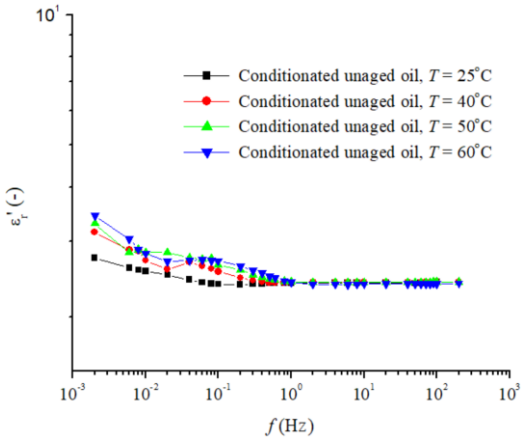

Fig. 6.7. The real part of the complex relative permittivity (ε_r') variation as a function of frequency for different measurement temperatures (unaged oil).

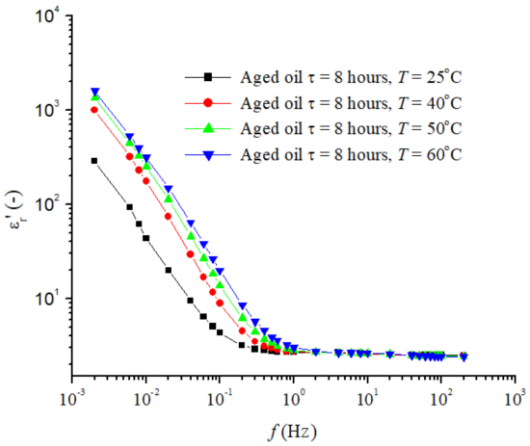

Fig. 6.8. The real part of the complex relative permittivity (ε_r') variation as a function of frequency for different measurement temperatures (oil aged 8 hours and aging applied voltage U = 13 kV).

As such, the value where ε_r' grows, or the point where the path modifies its slope, may be utilized to determine the relaxation frequency associated with the electric relaxation phenomenon. (See Fig. 6.3).

Figs. 6.7 and 6.8 show the real part of the complex relative permittivity for conditioned and aged oil at different temperatures respectively. Longer aging durations and higher measuring temperatures are shown to decrease the plateau region for the ε_r' variation with frequency (i.e., Fig. 6.3 for unaged oil from 0.04 Hz at 16 Hz for 8 hours aging period at 25^{o}C measurement temperature). This occurs most likely as a result of various charge carrier species generated during the aging process, as well as a decrease in the liquid density and the involvement of complicated processes that are likely to trigger polarizability to diminish with temperature. [6.9] According to Fig. 6.3's findings, aged oil exhibits incredibly high values of ε_r' when tested at mHz-range frequencies. As such, ε_r' can reach values ranging from a few hundred to even above one thousand for frequencies under a few mHz. Also, Figs. 6.8 reveal that within a similar frequency spectrum, the increases in measurement temperature from 25 ^{o}C to 60 ^{o}C cause an important rise in ε_r' for aged oil.

The electrode polarization phenomenon (also known as spatial polarization), which corresponds to the accumulation of mobile charge carriers on the boundary between the electrodes of the measuring cell and the oil tested under the effect of an electric field, might be the explanation for these huge values (an extremely high value which can't be explained with conduction relaxation processes). Thus, an electrical double layer develops at the interface, whereby the voltage that's applied drops rapidly and an important electrical polarization occurs [6.1, 6.10]. Nevertheless, the spatial polarization phenomenon develops if the free charge carriers' transit time among electrodes is shorter than the voltage half-period, allowing them to get to the opposite sign electrode and so make a spatial charge at the oil-electrode junction. This effect is often reserved for moderately or strongly conductive materials, according to published studies. Mineral oil in a good state (unaged), being a highly efficient insulator, normally is not in such a situation, as observed in all the plots. However, because mineral oil has ionic conduction mainly, it is plausible to assume that this phenomenon is primarily driven by free ions that develop in the oil as a consequence of partial discharges and a high-strength electric field.

Another essential aspect is relating to how the dielectric loss factor varies with electric field frequency for oil aged, measured at different temperatures (Figs. 6.9 - 6.10).

Thus, for frequency values between 10^{-2} to 10^{-1} Hz, it can be seen that depending on the aging duration, the shapes of the variation plots modify and the loss factor appears to reach a maximum value, after which it shows a small decrease. This happens due to the electrode polarization phenomenon effect, which causes a quick rise of ε_r' and, as a consequence, a decrease in the tgδ calculated values (the dielectric loss factor being expressed like tg $\delta = \varepsilon_r''/ \varepsilon_r'$).

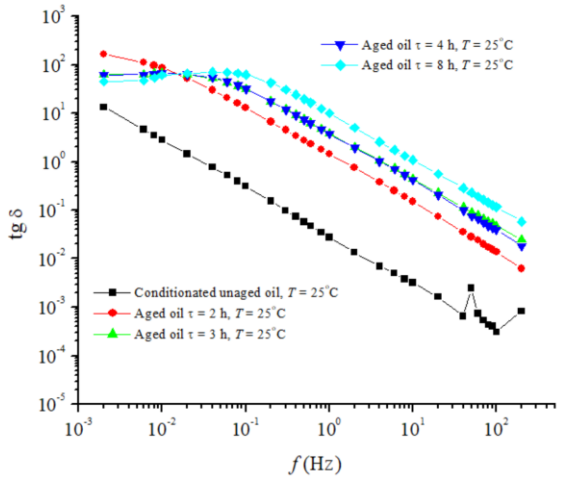

Fig.6.9. Variation of tg δ (dielectric loss factor) with frequency for various aging times (measurement temperature T = 25 ºC and (aging) applied voltage U = 13 kV).

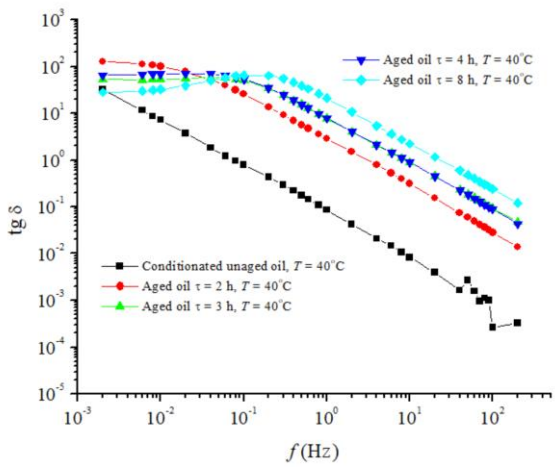

Fig.6.10. Variation of tg δ (dielectric loss factor) with frequency for various aging times (measurement temperature T = 40 ºC and (aging) applied voltage U = 13 kV).

6.3.2 Complex electrical modulus

As a way to more efficiently recognize and comprehend dielectric response (i.e., conduction), as well as to mitigate the polarization effect, the real and imaginary parts of the electric modulus will be studied, knowing that the electric modulus equates to the relaxation of the electric field in the dielectric material, thus facilitating us to detect associated phenomena related to the motion of electric charges [6.1].

The frequencies for which M'' presents maximum values at 40ºC measurement temperature (as an example) are presented in Table 6.1 and represent relaxation frequencies, where various species of charge carriers and polar free radicals are strongly relaxed (see Fig.6.11). This maximum value indicates that for all equivalent frequencies, charge carriers are most easily oriented in the electric field.

Table 6.1 Frequency corresponding to the $M''(f)$ peak at all tested aging periods and measurement temperature 40ºC

	M''	M''	M''	M''	M''
Aging time	(uo)	(2h)	(3h)	(4h)	(8h)
Peak freq. (Hz)	0.08	3	8	9	18

Also, all of the $M''(f)$ values show that the relaxation frequency increases with increasing aging time, a trend that can also be assigned, to the appearance of some species of polar free radicals whose relaxation happens at higher frequencies, meaning these polar radicals are capable of orienting more easily at these electric field frequencies (i.e., can ‘rotate more easily).

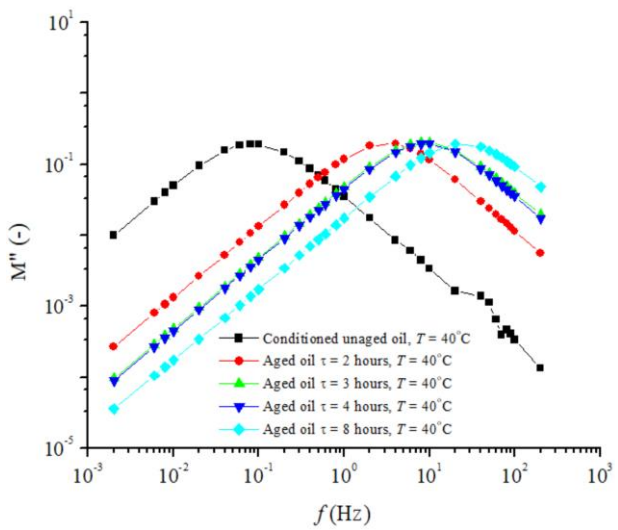

Fig.6.11. Electrical modulus (*M''*) imaginary component variation as a function of frequency for various aging times (measurement temperature T = 40°C and aging applied voltage U = 13 kV).

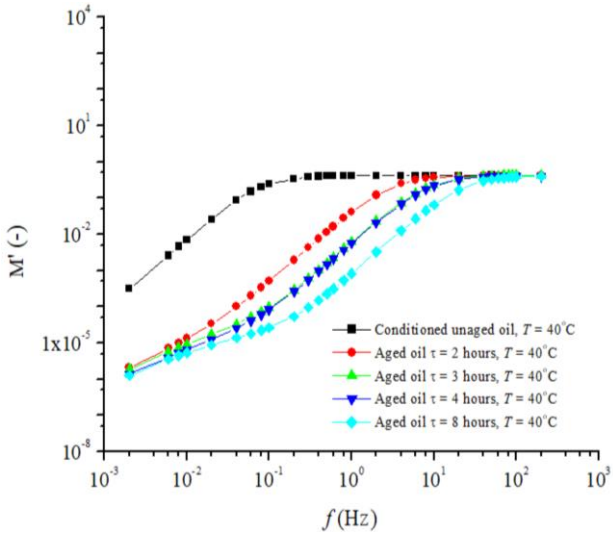

Fig.6.12. Electrical modulus (*M'*) real component variation as a function of frequency for various aging times (measurement temperature T = 40°C and aging applied voltage U = 13 kV).

Additionally, for *M'* variation with frequency, the same frequencies appear to trigger changes in the slopes of the curve; which are similarly influenced by the aging duration and measurement temperature. The frequency dependence of the real component of the electric modulus *M'* for various aging durations is shown in Fig. 6.12.

It can be seen that *M'* reduces to very low values at small frequencies, indicating that the electrode polarization influence has been eliminated [6.1]. As seen in Figs. 6.13 and 6.14, there is a significant temperature and aging duration dependency in the variation of *M''(f)* inflection point.

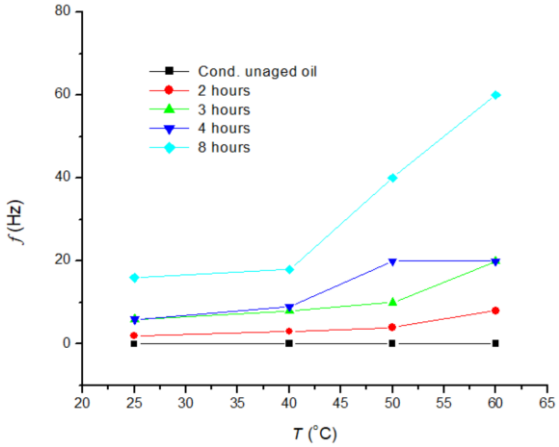

Fig. 6.13. Variation of the frequency corresponding to the peak point for *M''*(uo); *M''*(2h); *M''*(3h) *M''*(4h); M"(8h) as a function of the measuring temperature (measurement temperature T = 25; 40; 50; 60°C and aging applied voltage U = 13 kV).

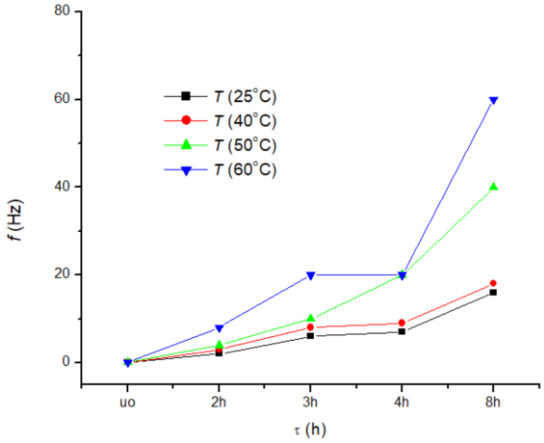

Fig.6.14. Variation of the frequency corresponding to the peak point for *M''*(uo); *M''*(2h); *M''*(3h) *M''*(4h); M"(8h) as a function of the aging time (measurement temperature T = 25; 40; 50; 60 °C and aging applied voltage U = 13 kV).

Plotting these values make the causal connection between these parameters more obvious; thus, such an increase is associated with the charge carriers' long-range mobility and also polar free radicals' quantity growth. Similar values for the same temperatures and aging times were observed for *M'(f)* variation. This significant change for aged oil reinforces the assumption that the subsequent polar free radicals and charge carriers in oil after aging orient more easily in electric fields, depending on species and concentrations.

6.3.3 Complex conductivity for mineral oil (MOL)

To better identify dielectric changes driven by the influence of the high-strength electric field and partial discharges, the real and imaginary components of the complex conductivity ($\sigma'$and σ'') were analyzed too. The results reveal a wide plateau in the measured frequency spectra of the real component of complex conductivity (σ') from 10^{-3} Hz to around 2 Hz, with the absolute value rising towards higher values as aging duration and measurement temperature increase as is displayed in Figs. 6.15-6.16.

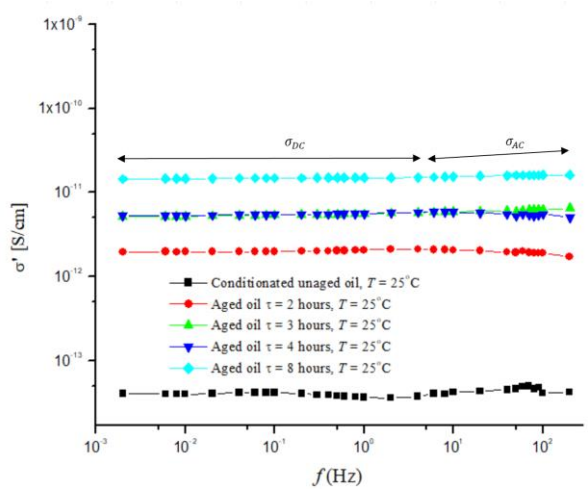

Fig.6.15. σ' variations as a function of frequency for various aging times (measurement temperature T = 25 ºC and aging applied voltage U = 13 kV).

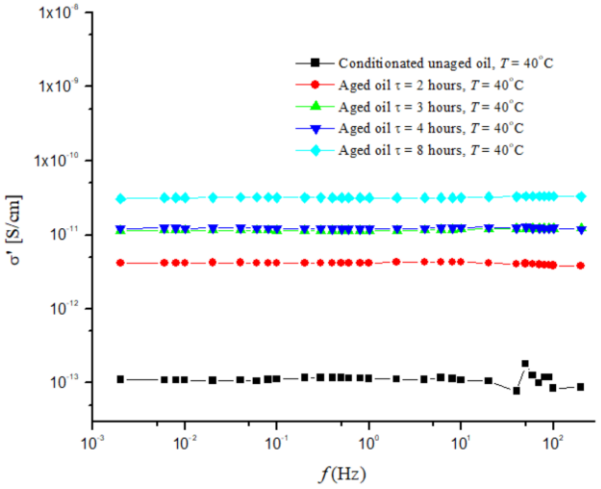

Fig.6.16. σ' variations as a function of frequency for various aging times (measurement temperature T = 40 ºC and aging applied voltage U = 13 kV).

Recalling that such a plateau where the real part of conductivity does not change with frequency defines DC conductivity i.e., σ_{DC}. The study reveals that at low frequencies, conductivity is produced by free conduction ion displacement over long distances, leading to charge transport between electrodes. The slope of the curves for aged oil samples show slightly changed (Fig. 6.15) at frequencies over 2 Hz, indicating that as frequency increases, $\sigma'(f)$ also increases. This happens due to the dissipative component of the conductivity $\sigma_{AC}(f)$, which appears additional, as a consequence, the ions move over short distances without reaching the electrodes, therefore there is no charge transit between them. Furthermore, the absence of σ" dispersion in the low-frequency spectrum for unaged oil (Fig. 6.17) indicates a lower amount of charge carriers if compared to the aged oil samples (Fig. 6.18).

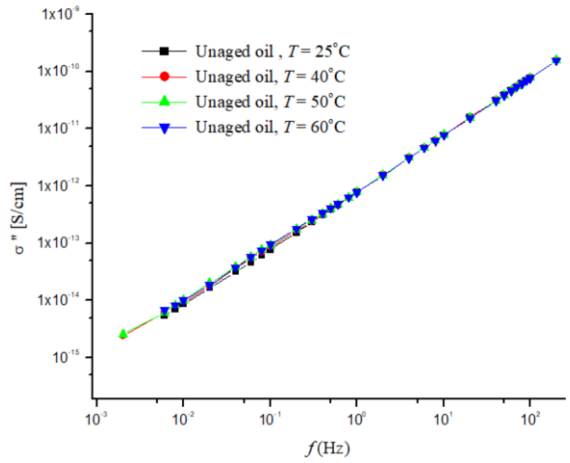

Fig.6.17. σ'' variations as a function of frequency at various temperatures for unaged oil sample.

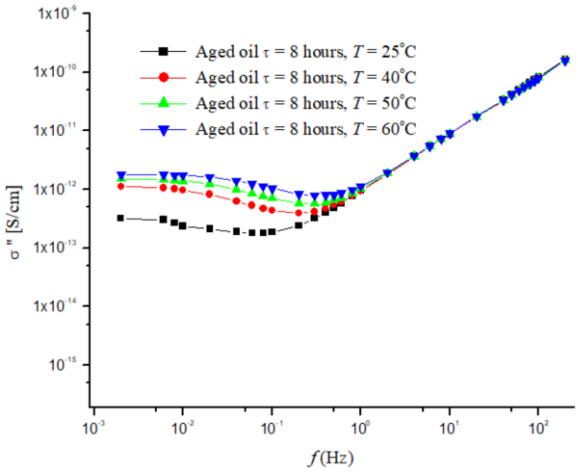

Fig.6.18. σ'' variations as a function of frequency at various temperatures for oil aged 8 hours.

This aspect being demonstrated also by the absence of electrode polarization phenomena for unaged samples, even in this (low) frequency range.

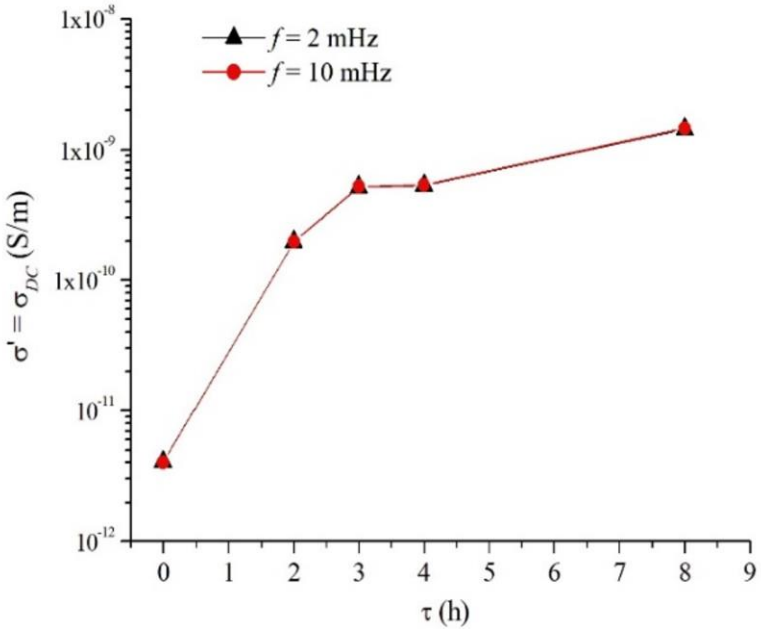

Fig. 6.19. σ_{DC} (real part of complex conductivity - σ', constant with frequency) variation as a function of aging duration for f = 2 and 10 mHz and T = 25 °C.

Per the data provided previously and generally acknowledging that σDC is equivalent to σ' at low frequencies (such as the range from 2 mHz to 2 Hz), Fig. 6.19 undoubtedly indicates that σ_{DC} grows with aging time duration, demonstrating that the concentration and potentially the mobility of conduction ions boost with aging period (τ).

6.3.4 Ionic mobility

Thinking of the possibility of higher mobility ions being generated with increasing aging duration (that might contribute to the huge increase in electrical conductivity by multiple orders of magnitude noted in Fig. 6.19), more focus will be put on estimating the average mobility of the free ions that participate in the conduction process.

With the guidance of the Tobazéon simplified model [6.11], it is possible to estimate the average mobility of free ions (μ_{ions}) relative to the frequency associated with the beginning phase of the electrode polarization phenomenon f_0. Relying on the fact that the values of the frequency f_0 correspond to the peak values of the $M''(f)$ plots in Fig. 6.11 and coincide with the inflection points of the $M'(f)$ slopes in Fig. 6.12 (that represent the relaxation time of the charge carriers - conduction ions in the oil samples, i.e., the electric field frequency at which the ions can move between the measuring cell's electrodes), it has been noticed that an extension of the aging period is reflected in a greater value of f_0 (Table 6.2).

As a result, the relaxation frequency f_0 of the conduction ions grows with aging duration, resulting in a decrease in relaxation time as the exposure duration to the action of the electric field and partial discharges rise. Figure 6.20 depicts the variation of the average mobility of conduction ions as a function of the aging period.

As anticipated, the mobility values (obtained through the above-simplified method) rise significantly with aging duration, from 10^{-7} m^2/Vs for unaged oil to 10^{-4} m^2/Vs for τ = 8 h.

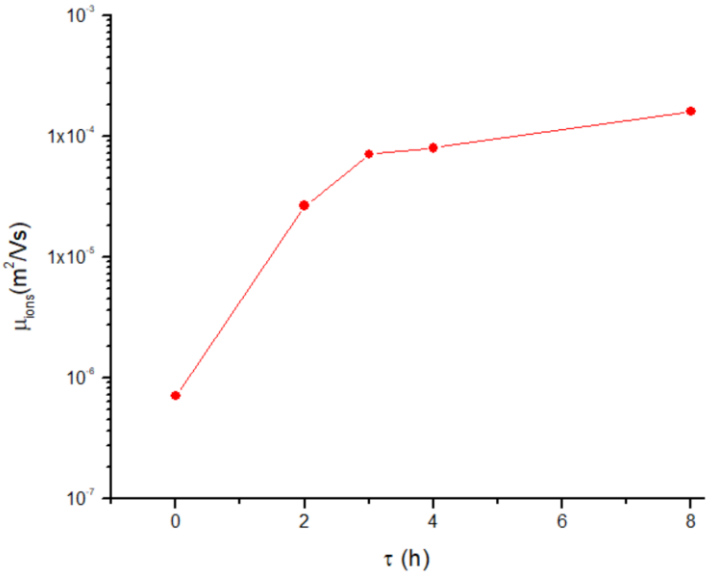

Fig. 6.20. Free ions average mobility variation as a function of τ - aging time at T = 40 °C.

In regard the method described above, the mean value of ion mobility obtained for unaged mineral oil at T = 40 °C (see Table 6.2) is around $3.55 \cdot 10^{-7}$ m^2/V·s, which is a greater value than those reported in the literature (~10^{-9} m^2/V·s) [6.12].

Table 6.2. Relaxation freq. (f_0) and ionic mobility (μ_{ions}) calculated for different aging durations at T = 40 °C

Temp. (° C)	Aging Time (hours)	f_0 (Hz)	μ_{ions} $(m^2 V^{-1} s^{-1})$
40 ° C	uo	0.08	7.10861E-07
40 ° C	2	3	2.66573E-05
40 ° C	3	8	7.10861E-05
40 ° C	4	9	7.99719E-05
40 ° C	8	18	1.599E-04

This occurs because the ionic mobility estimate is dependent on the relaxation frequency value of the conduction ions and is thus susceptible to calculation methods. Nonetheless, research has discovered comparable ion mobility values. As can be seen in Fig. 6.20, the results suggest that conduction ion mobility rises with longer aging periods. Therefore, extending the aging duration generates free-charge carrier species that have greater mobility (so very mobile ions). Consequently, the increase in the electric conductivity of aged oil may be attributed to the following factors: growth in conduction ion concentration as well as the generation of (new) charge carriers that have higher mobility.

6.3.5 Activation energy

The data reported above certainly show that electrical conduction in oil shifts significantly under the influence of the electric field and PDs. We went deeper into the reason for these conductivity shifts, which can be caused, on the one hand, by the increased concentration of free charge carriers led by the aging process and, on the other hand, as already demonstrated, by the generation of charge carriers that are more mobile and likely to participate in the conduction process. A possible solution to this quandary may be offered by the estimation of the average value of the activation energy E_a of the conduction ions. The activation energy is defined as the minimal amount of energy required for a free electrical particle (ion, etc.) to engage in the conduction process, namely, to become a free charge carrier capable of moving under the influence of an electric field. The graphical representation of $\log\sigma_{DC}$ as a function of $1/T$, shown in a straight line with a slope equivalent to $-E_a/k$, may be utilized for estimating the values of E_a.

Figure 6.21 displays the straight lines having slopes corresponding to $-E_a/k$, obtained by utilizing the values of σ_{DC} for the onset (0h), middle (4h), and end (8h) of the aging period. The average values of the activation energy for both unaged and aged mineral oil (MO) are provided in Table 6.3.

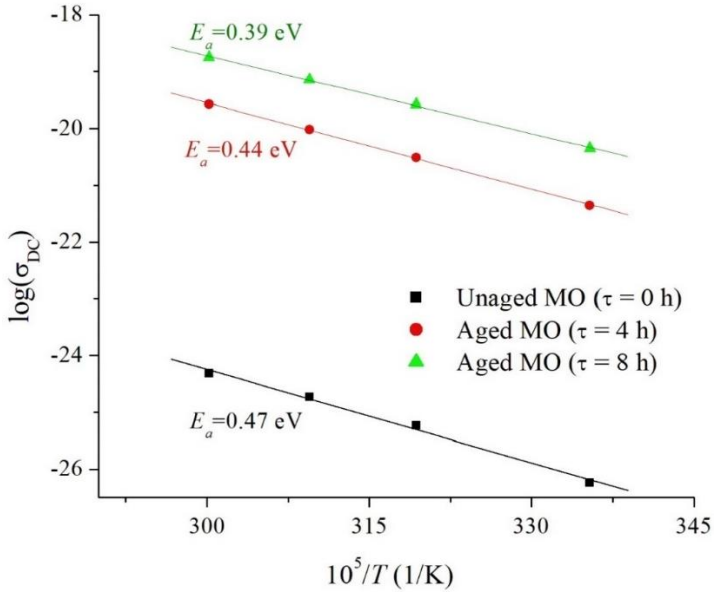

Fig. 6.21. Variation of unaged and aged MO static conductivity (σ_{DC}) with temperature represented in Arrhenius coordinates.

Table 6.3 Activation energy averages values for free charge carriers within unaged and aged mineral oil (MO)

MO sample	Unaged MO (τ = 0 h)	Aged MO (τ = 4 h)	Aged MO (τ = 8 h)
E_a (eV)	0.47	0.44	0.39

The estimated activation energy values are comparable with the ones presented in other past studies [6.1, 6.9]. The value displayed reveals that as oil ages, the activation energy of conduction ions decreases, indicating more aggressive degradation processes. Thus, we can say that as the aging duration increases, degradation processes become more aggressive, and as a result, the activation energy values drop (approximately 20% difference between unaged and 8-hour aged oil), reflecting that chemical reactions trigger a major fracture stage of the oil molecules. This confirms that increasing the aging time generates an increase in the concentration of free ions, alongside the emergence of new species of charge carriers that are more agile and sensitive to being engaged in the conduction process.

6.4 Influence of PD on the DC resistivity of transformer oil

The impact of partial discharges and high electric fields (accelerated electrical aging) on the electrical resistivity of mineral oil will be evaluated with the objective of conducting additional research from a different but complementary viewpoint.

Thus, a Keithley 6517B electrometer and an IRLAB CL-1 standard dielectric liquids cell were utilized to determine (at ambient temperature) the absorption and resorption currents of the oil samples. The measurements were conducted on five types of samples described in Table 6.4. Each of the samples was obtained by preconditioning Mol® mineral oil (MO) into a forced flow oven at T = 50 ºC for 72 h.

Table 6.4. Analised mineral oil samples.

Sample	Composition
MO cond.	150 ml unaged oil
MO1ml	150 ml unaged oil + 1 ml aged oil
MO2ml	150 ml unaged oil + 2 ml aged oil
MO3ml	150 ml unaged oil + 3 ml aged oil
MO4ml	150 ml unaged oil + 4 ml aged oil

The oil samples were obtained as follow: 150 ml of conditioned mineral oil was polluted with 1 ml, 2 ml, 3 ml, and 4 ml of accelerated aged oil, following the process described in Chapter 5 at 13 kV for 4 hours. To homogenize the mixture, the produced samples were put in hermetic glass bottles with a nitrogen pillow and then warmed to T = 50 ºC for 12 hours.

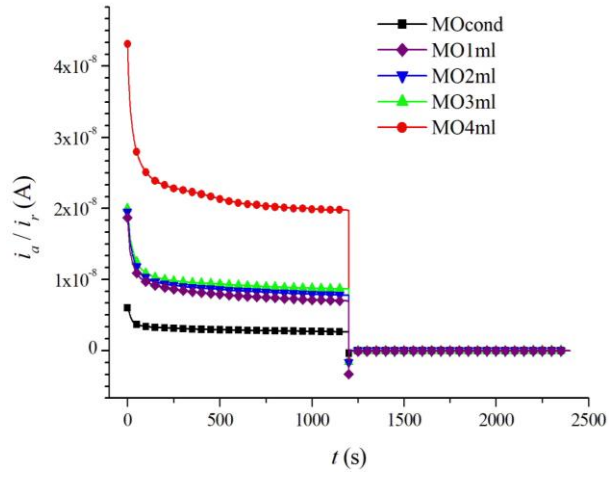

Fig. 6.22. Absorption and resorption currents variation with regard to the measurement duration (U_0 = 200 V and T = 24 ºC).

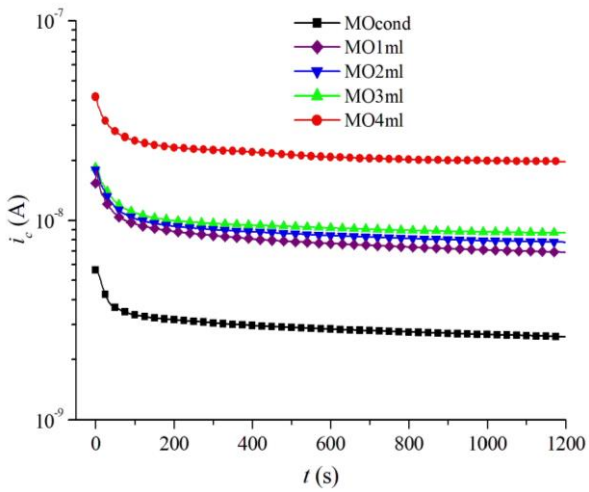

Fig. 6.23. Conduction current variation with regard to measurement time (U_0 = 200 V and T = 24 ºC).

Fig. 6.22 show what happens when conditioned mineral oil is contaminated with a very small amount of accelerated aged oil; thus, a significant increase in absorption and reabsorption currents is observed.

The results obtained reveal that $i_a(t)$ and $i_r(t)$ rise extensively when the add on aged oil volume grows from 1 ml (MO1ml) to 4 ml (MO4ml). So, as a consequence of contaminating the conditioned oil with a small amount of aged oil, the proportion of free charge carriers (ions) and electric dipoles increases, causing a rise in the absorption current components, particularly the conduction and polarization currents.

Into the Fig. 6.23 displays that the conduction current computed using $i_C(t) = i_a(t) - i_r(t)$, rises by an order of magnitude for the MO4ml sample as opposed to conditioned oil. With respect to the results shown in Fig. 6.23, the electrical resistivity of the examined oil samples has been computed by considering the dimensions of the dielectric liquid measuring cell.

Fig. 6.24a shows the findings for $i_c(60)$ and $i_c(600)$ – i.e., measured after 60 s and 600 s from the time of voltage application, with the corresponding electrical resistivity variation shown in Fig. 6.24b.

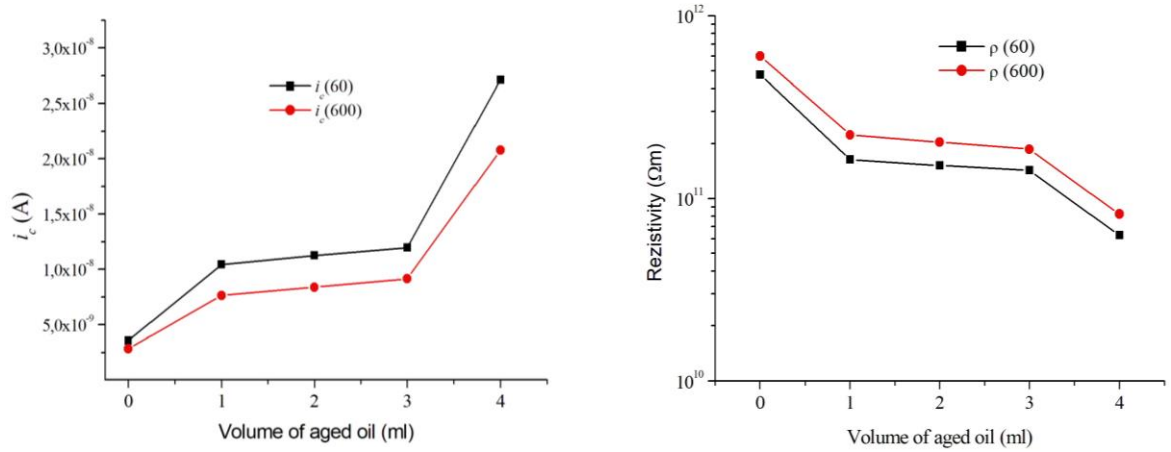

(a) **(b)**

Fig. 6.24. **a**) Variation of $i_c(60)$ and $i_c(600)$ as a function of aged oil volume; (**b**) Variation of ρ(60) and ρ(600) as a function of aged oil volume.

The findings reported previously clearly demonstrate that the absorption and resorption current plots and values are altered when conditioned mineral oil is contaminated with very small quantities of accelerated aged oil, subjected to high-strength electric fields and partial discharges. This is most likely caused by modifications in the polarization and conduction currents, brought on by the formation of free polar radicals and charge carriers throughout the aging process. This assumption is founded on the observation that modifications in absorption current curves appear both for short periods of time (t < 100 s) from the voltage application, which identifies the polarization phenomenon, and over longer periods of time (t > 100 s), which describes the conduction process [6.8]. Also, it is interesting to note that when 4 ml of aged oil is mixed with conditioned oil, the electric resistivity decreases by almost one order of magnitude relative to the conditioned oil. Considering that the accelerated aged oil volume only makes up 2.67% of the overall oil volume and that the aging duration is just 4 hours, this decrease is noteworthy, indicating a very high concentration of charge carriers in the aged oil.

GENERAL CONCLUSION, ORIGINAL CONTRIBUTIONS, AND FUTURE WORK

General conclusion

The primary conclusions of the investigation that support the study's goal confirm the significant impact of the high-strength electrical field and partial discharges on the mineral oil dielectric properties of the transformer. In light of this, mineral oil degradation caused by the high-strength electric field and PDs has been investigated based on a novel experimental technique that utilizes an original aging cell, employing the methods of dielectric response analysis in time and frequency. The suggested aging method for accelerated aging of transformer mineral oil is particularly important for evaluating the performance of the insulation system since it enables the estimation of the impact of electric fields and partial discharges on the oil state. Several aspects were addressed in the design of the aging cell and the experimental method, the most significant of those being the emergence of gas bubbles in the oil-induced by the action of a high-strength electric field. The initiation and ongoing preservation of an adequate quantity of partial discharges in the gas bubbles were then also considered.

Regarding the proposed aging technique, it can be concluded that it has been perfected and refined following careful observation of the aging phases (formation of gas bubbles, partial discharges, etc.), adapting it to the specific physical phenomena of the process along with the entire constructive solution of the cell.

Compared with ASTM D 6180 - 05, the experimental technique suggested in this study allows us to account for the true phenomenon of transformer operation, where local concentrations of electric field and PDs arise in oil quantity (owing to micro-defects and/or contaminants). Thus, the basic objective of the study, which was to establish an experimental method for electrical aging by generating gas bubbles in the oil volume and subsequently PDs, was successfully accomplished and implemented.

Regarding the acquired results, it can be confirmed that the proposed aging technique is reliable and efficient, providing repetitive and consistent results. The findings reported indicate an unusually high value of real and imaginary parts of the complex relative permittivity for the low-frequency range of the electric field, demonstrating, among others, the occurrence of the electrode polarization effect. However, the value obtained (order of magnitude 10^3) was not observed in the case of thermal aging, even for an extremely long aging time. Furthermore, it has been found that the electric conductivity of the mineral oil grows substantially for the aged oil samples (i.e., rises with aging duration). This happens because, as the oil ages, a large number of free charge carriers (including positive and negative ions) are produced and contribute to the conduction phenomenon.

Also, it was shown that the electrical resistivity of the contaminated oil was lowered by nearly one order of magnitude, although the quantity of aged oil blended with the conditioned oil

was less than 2.67% of the overall oil volume. All these factors point out that mineral oil properties deteriorate quickly under high-strength electric fields and PDs, most likely due to a significant density increase in the mobile charge carriers. It is worth pointing out that all research in the field acknowledges that the rise in the concentration of charge carriers and polar free radicals is a consequence of the electric stress impact.

Furthermore, a second probable hypothesis concerning the generation of different high mobility charge carriers has been investigated to explain the substantial growth of the conductivity value. Thus, the mean mobility of conduction ions was estimated for various aging periods and measurement temperatures by utilizing a simplified method (using the inflection point frequency values from the complex modulus graphs - *M'(f)* and *M''(f)*).

The research results unambiguously demonstrate that the appearance of free-charge carrier species with greater mobility is a result of longer aging durations. The existence of such free ions shows that the process of fragmentation of hydrocarbon molecules by the action of the electric field and partial discharges is an ongoing process that affects all chemical species in oil. Additionally, based on the estimation of the activation energy, it can be concluded that the growth of the oil's electric conductivity can be attributed, on the one hand, to a boost in the free charge carrier's concentration produced under the effect of the electric field and partial discharges, along with the emergence of new free charge carrier species that are more mobile and easily activated during the conduction process.

Original contributions

Regarding the original contributions, it can be mentioned that:

- A detailed examination of the available documentation was done on the general degradation processes brought on by the combination of partial discharges and high-strength electric field with transformer mineral oil. Evaluation of other elements that contribute to oil aging and the ensuing phenomenon was also undertaken.
- Another aspect of originality is the design and manufacturing of a novel original aging cell that generates continuous and monitored partial discharges in the oil volume (different than the ASTM D 6180-05 method), as well as the establishment of a specific methodology to execute accelerated electric aging.
- A numerical model was developed for two metallic electrode designs (three and six disks) and was applied to a Multiphysics study to analyze electric field distribution using the finite element method in the electrostatic regime.

- A detailed comparative study using dielectric spectroscopy was conducted. It assessed the state of aged and virgin mineral oil at different temperatures and aging times by measuring and computing the main diagnostic factors (complex relative permittivity, dielectric loss factor, complex conductivity, etc.). To gain a comprehensive understanding of the mechanisms influencing the rise in electrical conductivity, the main factors responsible for oil deterioration were identified and emphasized by measuring the absorption and resorption currents and computing the mobility of ions and their activation energy.
- It was demonstrated that large effect of electric aging on oil dielectric characteristics by employing samples contaminated with varying amounts of aged oil; even a tiny percentage of electric-aged oil considerably impairs the oil's properties.
- The research results were published in the following journal articles and conference papers from different scientific conferences and events:
    - **Manea A**., L.M. Dumitran, C., Borzea and E. Cazacu (2021) "ACCELERATED AGEING METHOD OF MINERAL OIL UNDER HIGH ELECTRIC FIELD AND PARTIAL DISCHARGES", 2021 12th International Symposium on Advanced Topics in Electrical Engineering (ATEE) [Preprint]. doi:10.1109/atee52255.2021.9425323. WOS:000676164800155, ISBN:978-1-6654-1878-2, ISSN:1843-8571
    - **Manea A.**, Gorjanu T, Lazeanu A. and Dumitran L.M. (2022) "Effect of electrical accelerated aging on DC resistivity of mineral oil used in power transformers", Energies, 16(1), p. 294. doi:10.3390/en16010294. WOS:000908927300001, eISSN:1996-1073,
    - L. Marius Dumitran, **Manea A**. and T. Gorjanu, (2023) "Influence of electrical accelerated aging on the conductivity and activation energy of free ions in mineral oil", 2023 13th International Symposium on Advanced Topics in Electrical Engineering (ATEE) [Preprint]. doi:10.1109/atee58038.2023.10108223. INSPEC Accession Number: 23002782
    - Dumitran L.M., **Manea A**. and Gorjanu T, (2023) "Effect of accelerated aging under high electric field and partial discharges on electric conduction in mineral oil", IEEE Transactions on Dielectrics and Electrical Insulation, 30(4), pp. 1623–1631. doi:10.1109/tdei.2023.3292804. INSPEC Accession Number: 23641592.
    - **Andrei Manea**, Laurentius-Marius Dumitran, Teodora Gorjanu, Claudia Borzea, "ON SOME COMPARISON BETWEEN ACCELERATED AGING OF MINERAL OIL UNDER HIGH ELECTRIC FIELD AND HIGH TEMPERATURE", APME, vol. 17, no. 1, pp. 44–51, Feb. 2022, Accessed: Jan. 03, 2024. [Online]. Available: https://journal.iem.pub.ro/apme/article/view/73 ISSN / ISSN-L: 1843-5912, CROSSREF https://www.doi.org/10.36801/apme.2021.1.6

Future work

The following perspective for further research is suggested in light of the completed investigations in the current PhD thesis:

- Future research will focus on evaluating the influence of different parameters in the aging process of transformer oil, such as temperature, frequency, or applied voltage.
- Carrying out the aging process for various oil types, such as vegetal or synthetic, to compare and analyze the dielectric properties of the oils.

GENERAL BIBLIOGRAPHY

[1.1] A. Beroual, U. Khaled, P. Mbolo Noah and H. Sitorus, "Comparative Study of Breakdown Voltage of Mineral, Synthetic and Natural Oils and Based Mineral Oil Mixtures under AC and DC Voltages," Energies, Vol. 10, no. 4, p. 511, 2017.

[1.2] G. J. Pukel, R. Eberhardt, H. M. Muhr, F. Baumann and W. Lick, "Large Power Transformers for Alternative Insulating," Proceedings of the 16th International Symposium on High Voltage Engineering, Innes House, Johannesburg, paper F-27, pp 1-4, 2009.

[1.3] M. Wang, A.J. Vandermaar, K.D. Srivastava, "Review of condition assessment of power transformers in service," IEEE Electr. Insul. M., Vol. 18 no. 6, pp. 12–25, 2002.

[1.4] M. Darveniza, T.K. Saha, D.J. Hill, T.T. Le, "Investigation into effective methods for assessing the condition of insulation in aged power transformers," IEEE Trans. Power. Delivery., Vol. 13, Issue 4, pp. 1214-1223, October 1998.

[1.5] S.M. Gubanski, P. Boss, G. Csepes, V. Der Houhanessian, J.C. Filippini, P. Guuinic, et al., "Dielectric response methods for diagnostics of power transformers," IEEE Electr. Insul. M., Vol. 19, Issue 3, pp. 2-17, May-June 2003.

[1.6] T.K. Saha, "Review of modern diagnostic techniques for assessing insulation condition in aged transformers," IEEE Trans. on Dielect. and Electr. Insul., Vol. 10, Issue 5, pp. 903–917, October 2003.

[1.7] A. Bouaïcha, I. Fofana, M. Farzaneh, A. Setayeshmehr, H. Borsi, E. Gockenbach, et al., "Dielectric spectroscopy techniques as quality control tool: a feasibility study," IEEE Trans. on Dielect. and Electr. Insul., Vol. 25, Issue 1, pp. 6-14, January-February 2009.

[1.8] M.H. Meshkatoddini, "Aging study and lifetime estimation of transformer mineral oil," Am. J. Eng. Applied. Sci., Vol. 4, no. 1, pp. 384-388, 2008

[1.9] *Standard test method for stability of insulating oils of petroleum origin under electrical discharge*, ASTM D 6180 – 05, 10(3):6180, 2005.

[2.1] Harlow, J., 2004. Electric power transformer engineering. Boca Raton, Fla.: CRC Press.

[2.2] Bureau, E. et al. (2022) Various types of transformer core assemblies: Video tutorial, Electronics For You. Available at: https://www.electronicsforu.com/videos-slideshows/videos/transformer-core-assemblies-types (Accessed: 29 November 2023).

[2.3] Bestoptek.com. 2022. Bestop Technologies. [online] Available at: <http://www.bestoptek.com/Support-Transformer-Basic.html> [Accessed 13 July 2022].

[2.4] Paper (2018) Smit Draad / Draad Nijmegen B.V. Available at: https://smitdraad.nl/paper-covered-wire/ (Accessed: 04 December 2023).

[2.5] How online transformer monitoring can empower asset managers working from home et al. (no date) Transformer insulation, Insulect. Available at: https://insulect.com/products/transformer-insulation (Accessed: 04 December 2023).

[2.6] L.M. Dumitran, "Sisteme de izolaţie electrică", Editura Printech, Bucureşti, 2008.

[2.7] P.V. Noţingher, Sisteme de izolaţie, Editura Printech, Bucureşti, 2002.

[2.8] [Megger.com. 2022. Electrical test equipment application solutions from Megger. [online] Available at: <https://megger.com/applications/transformers/transformer-insulation> [Accessed 20 July 2022].]

[2.9] M. Koch and T. Prevost, „Analysis of Dielectric Response Measurements for Condition Assessment of Oil-Paper Transformer Insulation", IEEE Transactions on Dielectrics and Electrical Insulation", Vol. 19, No. 6, 2012, pp. 1908 – 1915.

[3.1] P.V. Noţingher, Sisteme de izolaţie, Editura Printech, Bucureşti, 2002.

[3.2] Tera Analysis Ltd.- QuickField software providers for electromagnetic, heat transfer and stress analysis. M. design applications: electrical machines (no date) Electric field stress in the transformer oil, QuickField.com. Available at: https://quickfield.com/advanced/transformer_electric_stress.htm (Accessed: 04 December 2023).

[3.3] W. J. K. Raymond, H. A. Illias, A. H. A. Bakar, and H. Mokhlis, "Partial discharge classifications: Review of recent progress," Meas. J. Int. Meas. Confed., vol. 68, no. February, pp. 164–181, 2015.

[3.4] Overview and partial discharge analysis of Power Transformers: A ... Available at: https://ieeexplore.ieee.org/document/9411852/ (Accessed: 07 December 2023).

[3.5] B. Karthikeyan, S. Gopal, and S. Venkatesh, "ART 2-an unsupervised neural network for PD pattern recognition and classification," Expert Syst. Appl., vol. 31, no. 2, pp. 345–350, 2006.

[3.6] Sun, C.C. et al. (2020) 'Research on the temperature rise characteristics of power transformers based on fluid-solid-thermal coupling', Journal of Physics: Conference Series, 1601(2), p. 022017. doi:10.1088/1742-6596/1601/2/022017.

[3.7] ***IEEE C57.95/1991 Guide for Loading Mineral-Oil-Immersed Transformers

[3.8] E. Jezierski, Z. Gogolevski, Z. Kopczynski, J. Szmit, Transformatoare electrice – constrictie si proiectare , Editura tehnica , Bucuresti,1996.

[3.9] I. Fofana, J. Sabau, D. Bussieres and E. B. Robertson, "The mechanism of gassing in power transformers," 2008 IEEE International Conference on Dielectric Liquids, 2008, pp. 1-4, doi: 10.1109/ICDL.2008.4622489.

[3.10] M.H. Meshkatoddini, "Aging study and lifetime estimation of transformer mineral oil", Am. J. Eng. Applied. Sci., Vol. 4, no. 1, pp. 384-388, 2008.

[3.11] J. Hill, Z. Wang, Q. Liu, C. Krause, and G. Wilson, "Analysing the power transformer temperature limitation for avoidance of bubble formation", IET High Voltage J., Vol. 4, Issue. 3, pp. 210-214, 2019.

[3.12] I. Fofana, A. Bouaicha, M. Farzaneh, and J. Sabau, „Ageing Behavior of Mineral and Ester Liquids: A Comparative Study", 2008 Annual Report Conference on Electrical Insulation Dielectric Phenomena (CEIDP), , Quebec, 26-29 October 2008, pp. 87-90

[4.1] L.V. Badicu, "Diagnosis and monitoring of insulation systems of power transformers," PhD dissertation, Dept. of Electr. Eng., University Politehnica of Bucharest, 2011.

[4.2] **Manea, A. et al. (2022) 'Effect of electrical accelerated aging on DC resistivity of mineral oil used in power transformers', Energies, 16(1), p. 294. doi:10.3390/en16010294.**

[4.3] Jonscher, A.K. (1996) Universal relaxation law: A sequel to dielectric relaxation in solids. London: Chelsea Dielectrics Press.

[4.4] (No date) Cursul 8-9. Polarizarea electric ă a Izola iilor - pub.ro. Available at: http://www.elmat.pub.ro/~dumitran/Sisteme%20de%20izolatie/Note%20de%20curs/Cursul%208-9.pdf (Accessed: 19 December 2023).

[4.5] ''Novocontrol Technologies, WinDETA 5.65-owner's manual,'' nr.9,20007

[4.6] Bakar, N., Abu-Siada, A. and Islam, S. (2014) "A review of dissolved gas analysis measurement and interpretation techniques," IEEE Electrical Insulation Magazine, 30(3), pp. 39–49. Available at: https://doi.org/10.1109/mei.2014.6804740.

[5.1] M.H. Meshkatoddini, "Aging study and lifetime estimation of transformer mineral oil", Am. J. Eng. Applied. Sci., Vol. 4, no. 1, pp. 384-388, 2008.

[5.2] Standard test method for stability of insulating oils of petroleum origin under electrical discharge, ASTM D 6180 – 05, 10(3):6180, 2005.

[5.3] Manea, A. et al. (2022) "Effect of electrical accelerated aging on DC resistivity of mineral oil used in power transformers," Energies, 16(1), p. 294. Available at: https://doi.org/10.3390/en16010294.

[5.4] **Marius Dumitran, L., Manea, A. and Gorjanu, T. (2023) "Influence of electrical accelerated aging on the conductivity and activation energy of free ions in mineral oil," 2023 13th International Symposium on Advanced Topics in Electrical Engineering (ATEE) [Preprint]. Available at: https://doi.org/10.1109/atee58038.2023.10108223.**

[6.1] Kremer, F. and Schönhals, A. (2012) Broadband dielectric spectroscopy. Berlin; Heidelberg: Springer.

[6.2] F Ciuprina,"Caracterizarea dielectricilor Solizi Prin Spectroscopie Dielectrica". Available at: http://www.elmat.pub.ro/~florin/student/Master-MDE/Spectroscopie%20dielectrica.pdf (Accessed: 22 May 2023).

[6.3] **Marius Dumitran, L., Manea, A. and Gorjanu, T. (2023) 'Influence of electrical accelerated aging on the conductivity and activation energy of free ions in mineral oil', 2023 13th International Symposium on Advanced Topics in Electrical Engineering (ATEE) [Preprint]. doi:10.1109/atee58038.2023.10108223.**

[6.4] Dumitran, L.M. et al. (2014) "Method for lifetime estimation of power transformer mineral oil," Fuel, 117, pp. 756–762. Available at: https://doi.org/10.1016/j.fuel.2013.10.002.

[6.5] A.K. Jonscher, "The Universal Dielectric Response,", Nature, 267, 1977, pp. 673-679.

[6.6] A.K. Jonscher, "The Universal Dielectric Response: A Review of Data and their New Interpretation", Phys. Thin. Films, 11, 1980, pp. 205-317.

[6.7] J. Brunson, Hoping conductivity and charge transport in low-density polyethylene, Ph.D., Utah State University, Logan, Utah, 2010.

[6.8] L.V. Badicu, "Diagnosis and monitoring of insulation systems of power transformers," PhD dissertation, Dept. of Electr. Eng., University Politehnica of Bucharest, 2011.

[6.9] Sidambarompoulé, X., Notingher, P., Paillat, T., Laurentie, J. and Leblanc, P., 2022. Study of electrical properties and estimation of average mobility and diffusion coefficients in several insulating liquids by dielectric spectroscopy. [online] Hal.archives-ouvertes.fr. Available at: <https://hal.archives-ouvertes.fr/hal-03224002> [Accessed 11 June 2022].

[6.10] C.P. Ganea, "Electrode polarization and interface effects in liquid crystal systems with mobile ions: development of a model of bipolar diffusion," Cent. Eu. J. of Physics, Vol. 4, no. 11, pp. 497-511, 2013.

[6.11] R. Tobazéon, Etude des phénomènes d'interface au contact d'un liquide isolant et d'un solide, Ph.D. dissertation, Université de Grenoble, 1973.

[6.12] M. Butcher, et al., "Conduction and breakdown mechanisms in transformer oil," IEEE Trans. Plasma Sci., vol. 34, no. 2, pp. 467–475, 2006.